universität wien

MASTERARBEIT

Titel der Masterarbeit

„Geometric Phase Transitions in Periodic Boundary Conditions“

Verfasserin ODER Verfasser

Clemens Moritz, BSc

angestrebter akademischer Grad

Master of Science (MSc)

Wien, 2014

Studienkennzahl lt. Studienblatt:	A 066 876
Studienrichtung lt. Studienblatt:	Masterstudium Physik
Betreuerin / Betreuer:	Univ.-Prof. Mag. Dr. Christoph Dellago

Zusammenfassung

Geometrische Phasen finden sich in Systemen, in denen Phasenseperation stattfindet. Sie sind charakterisiert durch das Auftreten von Tropfenformen die nicht sphärisch sind, ein Phänomen das durch die Verwendung von periodischen Randbedingungen ermöglicht wird. In dieser Arbeit wurden Computersimulationen anhand des 2D Ising Modells durchgeführt, um den Mechanismus des Übergangs von einer Scheibe zu einem Rechteck und des Kondensations-/Evaporationsübergangs zu untersuchen. Dabei wurden analytische Modelle sowie Ordnungsparameter und Reaktionskoordinaten entwickelt, deren Gültigkeit durch sogenannte Kommitorrechnungen verifiziert wurden.
Augenmerk wird auf die Rolle der Oberflächenspannung beim Kondensations-/Evaporationsübergang durch den Vergleich mit analytischen Modellen, die nach den Prinzipien der klassischen Nukleationstheorie entwickelt werden, gelegt. Weiters kommen wir zum Ergebnis, dass dieser Übergang durch die Größe des größten Clusters gut beschrieben ist und durch die Hinzunahme von zusätzlichen Parametern die Beschreibung nicht signifikant verbessert werden kann.
Für den Übergang von einem scheibenförmigen zu einem rechteckigen Cluster wurden kontinuierliche Ordnungsparameter und eine Reaktionskoordinate entwickelt, die uns Auskunft über den Fortschritt des Übergangs gibt. Des Weiteren wird ein Modell des Übergangs, das aus einer Abfolge von elliptischen Clustern konstruiert wird, behandelt.

Abstract

Geometric phases are found in systems which exhibit phase separation and are characterized by droplet shapes other than spherical that are stabilized by the use of periodic boundary conditions in simulations. In this work, we used computer simulations, employing the 2D Ising model as a toy model, to investigate the transition mechanisms of the disk-slab transition and the evaporation/condensation transition by doing analytic calculations and by developing order parameters and reaction coordinates which we validated using commitor calculations.
The role of the surface tension in the evaporation/condensation transition is investigated by comparing analytical considerations along the lines of classical nucleation theory to results obtained from Monte Carlo simulations. Furthermore, we found the transition to be described well by the size of the drop alone while the addition of other parameters does not yield a significant improvement.
For the slab-disk transition we have developed continuous order parameters as well as a reaction coordinate based on a Fourier transform that describes the progress of the transition. Moreover a transition model based on a succession of ellipses is used to estimate the excess surface of the cluster during the transition.

Danksagung

Diese Arbeit ist der vorläufige Abschluss meines Physikstudiums, das ich in den letzten sechs Jahren betreiben durfte. In dieser Zeit konnte ich das Leben als Student in Wien genießen, ein Umstand den ich einigen Menschen verdanke, die ich hier erwähnen möchte.
Zuallererst bedanke ich mich bei Prof. Christoph Dellago, der es mir ermöglichte diese Arbeit im Rahmen der Gruppe für computergestützte Physik zu verfassen, und Dr. Andreas Tröster für die Ideen und Daten die er zu diesem Projekt beigesteuert hat. Ich möchte auch allen Mitgliedern der Gruppe für computergestützte Physik dafür danken, dass sie mich über das letzte Jahr aufgenommen haben und mich mit ihrem Wissen und ihrer Erfahrung auf diesem Gebiet unterstützt haben.
Weiters danke ich den unzähligen Studienkollegen die ich heute zu meinen Freunden zählen darf, ohne deren Unterstützung dieser Abschluss nicht nur schwieriger gewesen, sondern auch der Spaß am und rundherum ums Studium zu kurz gekommen wäre.
Zu guter Letzt danke ich meiner Familie und insbesondere meinen Eltern, ohne deren moralische und finanzielle Unterstützung ein Studium in der Form, in der ich es leben durfte, nicht möglich gewesen wäre und meinem Vater, von dem ich von früh an die Begeisterung für Naturwissenschaft und für Physik im Speziellen vorgelebt bekommen habe. Ich danke euch dafür, dass ihr mich immer bedingungslos unterstützt habt!

Contents

1. Introduction

When we try to simulate molecular systems we are confronted with a fundamental problem: the number of molecules that make up the macroscopic materials we see around us and whose properties we want to simulate is on the order of 10^{23} or more. However, computer simulations can only be done at a much smaller size ranging from a couple of hundred to trillions of particles which have been achieved using supercomputers (see Eckhardt et al. [1] for an example). Furthermore one often wants to simulate over long time scales making it even more desirable to use smaller systems.
However, changing the size of a system also changes the physics. One obvious source of such problems are the interfaces introduced by the finite box we simulate in. If we think of a three dimensional, homogeneous, cubic system the fraction of particles that find themselves on the surface of the cube scales like

$$Q_S \sim \frac{V^{2/3}}{V} = V^{-1/3}, \tag{1.1}$$

meaning that if we consider a system with 1000 particles we will find around 50% of them on the surface while in a macroscopic system we expect this number to be orders of magnitude smaller. This, of course, significantly distorts any expectation values we want to gather from such a simulation [2].
To overcome these limitations usually one uses a trick known as toroidal or *periodic boundary conditions* (PBC). This means that we identify the walls of the box that are opposite to each other in such a way that a molecule that leaves the box through one wall at the same time enters the box through the opposite side. Interactions between particles are calculated by always choosing the closest "image" of a particle when doing the calculations (this procedure is known as *nearest image convention*). Given that there are no interactions of any kind (including long range correlations) that have a longer range than the length of the simulation box we can then hope that the system behaves as if it were embedded into a larger bulk system.
However, removing the interface at the box wall has some side effects when we try to simulate situations that involve boundaries between phases such as the formation of droplets from vapor. The growth of a drop from vapor in a system can be thought of as a competition between the cost that is involved in forming a boundary between the two phases and the advantage that the system can go to preferable configurations in each of the phases while still achieving the extensive constraint imposed on the system (such as the volume or pressure).
Given a fixed volume, the smallest surface that encloses that volume is a sphere. However, by using periodic-boundary conditions we give a sufficiently large enough drop within the system another way of minimizing its surface: by forming a cylinder or even a slab that is

in contact with the walls of the simulation box. Since atoms at the box walls are actually interacting with atoms from the other side of the box physically there is no surface and therefore there is no energetic cost associated with forming such a surface.
This behavior can be observed in any system that exhibits phase separation. As an example, figure 1.1 shows snapshots of a Lennard-Jones fluid simulated at different densities and a temperature chosen such that the system is within the gas-fluid coexistence region. The simulation is performed using periodic boundary conditions (PBC) in all directions and one can clearly see that the drop changes its shape from a ball to a cylinder and eventually to a slab. If we go to even higher densities we observe a similar sequence however liquid and gas switch their roles (i.e. eventually we see a spherical bubble inside the liquid bulk).

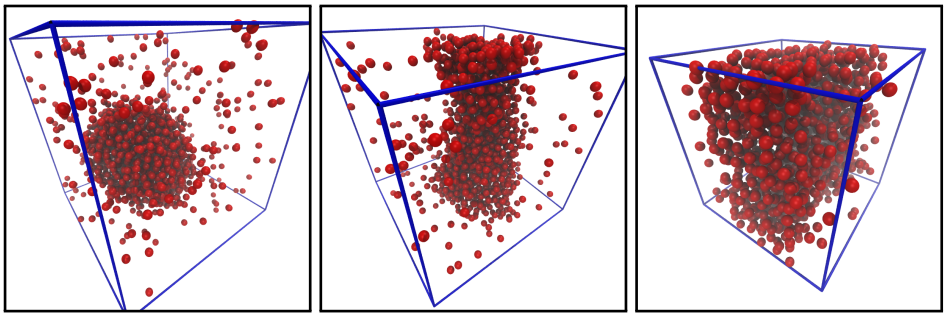

Figure 1.1.: Examples of geometric phases observed in a Lennard-Jones system with varying densities at reduced temperature 0.8. From left to right one sees a spherical, a cylindrical and a slab configuration found at reduced densities of 0.1, 0.15 and 0.4 respectively. The blue lines indicate the edges of the periodic box.

In a more accurate language, these changes of shape of the cluster manifest themselves as first order phase transitions when doing simulations within coexistence regions. They pose a significant challenge to various free energy sampling algorithms since they form free energy barriers that are orthogonal to the sampling coordinates and can slow down the sampling of such methods exponentially [3].
In this work we study the phase transitions between these geometric phases using the 2D Ising model as an example. Particular attention is paid to finding suitable reaction coordinates that will hopefully help us understand the dynamics of these transitions and their impact on free energy calculations.

2. The 2D - Ising Model

2.1. Definition and properties of the infinitely large system

To study the issue of geometric phase transitions we used a very simple form of the 2D Ising model, first proposed by Ernst Ising and Wilhelm Lenz in 1924 [4]. It consists of a set of spins σ_i that can take the values $+1$ or -1 and are located on a quadratic lattice. The energy of a system of N spins is given by

$$\mathcal{H} = -J \sum_{<i,j>} \sigma_i \sigma_j + h \sum_{i=1}^{N} \sigma_i, \tag{2.1}$$

where J is a coupling constant, $\sum_{<i,j>}$ indicates a summation over all nearest neighbor pairs and h is an external magnetic field.
In the limit of temperature $T \to \infty$ the spins decouple and the net magnetization of the system is 0. Furthermore, it was shown early on by Peierls [5] that at low temperatures this system will show spontaneous magnetization. Various approximate solutions [6, 7] describing this spontaneous magnetization were found before Onsager was able to derive an exact expression for the free energy, the specific heat and the internal energy [8].
Consistent with a second order phase transition at a critical temperature T_c, given by

$$T_c = \frac{2}{\ln(1 + \sqrt{2})} \frac{J}{k_B}, \tag{2.2}$$

where k_B is Boltzmann's constant, the specific heat diverges proportional to $-\log(|T - T_c|)$ while the internal energy per spin U is continuous at $T = T_c$.
The absolute value of the spontaneous magnetization per spin m, defined by

$$m = \frac{1}{N} \sum_{i=1}^{N} \sigma_i, \tag{2.3}$$

was computed by Yang [9] to be

$$m = \begin{cases} \left[1 - \sinh^{-4}(2\beta J)\right]^{1/8} & \text{for } T < T_c \\ 0 & \text{for } T \geq T_c \end{cases}, \tag{2.4}$$

where $\beta = \frac{1}{k_B T}$. Figure 2.1 shows a plot of $m(T)$. At a temperature T and in absence of a magnetic field the infinitely large system will exhibit a mean magnetization of plus or

minus $m(T)$. There is a vast amount of analytic results available for the Ising model which we will not quote in its entirety, however we list a few properties which will be relevant for our discussion. All of them are to be understood in the limit of infinite system size.

- The surface tension for a boundary between two regions with opposite magnetization that has no curvature is given by [8]

$$\sigma_0(\beta) = 2J + \log(\tanh(\beta J))/\beta. \tag{2.5}$$

- The interfacial free energy per unit volume of an ideal droplet (i.e. the droplet with minimal surface free energy) is given by

$$f_S = 2\sqrt{W}, \tag{2.6}$$

  where W is the volume bounded by the Wulff equilibrium shape [10] which can be expressed as the integral [11]

$$W = \frac{4}{\beta^2} \int_0^{\beta\sigma_0} \mathrm{d}x \, \cosh^{-1}\left(\frac{\cosh^2(2\beta J)}{\sinh(2\beta J)} - \cosh(x)\right). \tag{2.7}$$

In the form presented here the Ising Model is a very simple model that shows ferromagnetic behavior. Alternative interpretation of the quantities involved allows one to use the same model as a model for a gas or a binary alloy [2].

2.2. Monte Carlo simulations of the Ising Model

2.2.1. Metropolis Monte Carlo

Simulations in this work were carried out using a Metropolis Monte Carlo scheme [12] which will be described briefly in this chapter. The expectation value of a variable $A(\{\sigma_i\})$ in the canonical ensemble is given by

$$\langle A \rangle = \frac{\sum_{\{\sigma_i\}} A(\{\sigma_i\}) \, e^{-\beta\mathcal{H}(\{\sigma_i\})}}{\sum_{\{\sigma_i\}} e^{-\beta\mathcal{H}(\{\sigma_i\})}} \tag{2.8}$$

where $\sum_{\{\sigma_i\}}$ denotes the sum over all possible spin configurations $\{\sigma_i\}$. If we can produce a sample $\{\zeta_1\}, \{\zeta_2\}, \ldots, \{\zeta_{N-1}\}, \{\zeta_N\}$ from the unnormalized canonical probability density given by the values $e^{-\beta\mathcal{H}(\{\zeta_i\})}$, an estimate for the expectation value is given by

$$\langle A \rangle \approx \frac{1}{N} \sum_{i=1}^{N} A(\{\zeta_i\}). \tag{2.9}$$

To obtain a sample with a reasonable amount of computation the following scheme is used [12]:

1. Pick a trial move (discussed separately).
2. Calculate the difference in energy $\Delta U = \mathcal{H}_\mathrm{f} - \mathcal{H}_\mathrm{i}$, where $\mathcal{H}_\mathrm{f}$ and $\mathcal{H}_\mathrm{i}$ are the energy of the final and the initial state respectively.
3. Do an acceptance test.
   - If $\Delta U \leq 0$ accept the move.
   - If $\Delta U > 0$ accept the move with probability $e^{-\beta \Delta U}$.
4. If the move is accepted, add the new configuration to the sample, otherwise add the last accepted configuration to the sample again.

Two basic types of simulations have been performed: simulations where the magnetization fluctuates and simulations at fixed magnetization.

2.2.2. Trial Moves

For simulations where the magnetization is not fixed, simple spin flip moves were used. This means a spin on the lattice is picked at random and its direction is switched. The energy difference that is caused by this flip is solely dependent on the state of the four neighboring spins. In particular, if p is the number of spins that are parallel to the chosen spin before the flip, the energy difference is given by

$$\Delta U = 2J(2p - 4) \text{ with } 0 \leq p \leq 4. \tag{2.10}$$

These four values can be computed in advance and are looked up during the simulation.
Figure 2.1 compares the mean magnetization obtained using this Metropolis Monte Carlo scheme at different temperatures to the exact solution and shows that the two agree very well for low temperatures. Around the critical temperature, however, the finite size of the system produces significant deviations.
For simulations at constant magnetization (i.e. constant number of spins with value +1) spin exchange moves were used, where we propose to exchange two spins that have been chosen randomly. We will distinguish between two types of simulations; those with non-local dynamics where the spin pairs are chosen randomly from the whole system and those where only pairs of neighboring spins will be exchanged, resulting in local dynamics. The latter kind of spin-exchange move is also known under the name Kawasaki dynamics [13]. If the two chosen spins have the same orientation, the energy difference is 0. Otherwise the energy difference can again be expressed by the number of parallel spins in the neighborhood of each of the chosen spins, however two cases have to be distinguished (let p_1 and p_2 be the number of parallel spins in the vicinity of spin 1 and spin 2 respectively):

- The two spins are neighbors of each other. In this case the energy difference amounts to

$$\Delta U = 4J(p_1 + p_2 - 3) \text{ with } 0 \leq p_1, p_2 \leq 3. \tag{2.11}$$

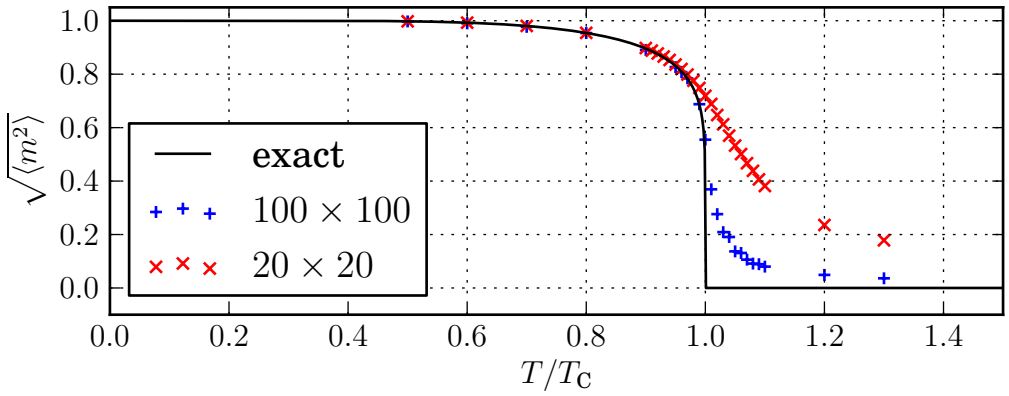

Figure 2.1.: Comparison of the exact expression for the spontaneous magnetization m as a function of temperature T to results obtained using Metropolis Monte-Carlo simulations on lattices of two different sizes. T_C is the critical temperature given by (2.2).

- If the two spins are not neighboring the energy difference is given by

$$\Delta U = 4J(p_1 + p_2 - 4) \text{ with } 0 \leq p_1, p_2 \leq 4. \tag{2.12}$$

With local dynamics only the first case applies.

3. Calculation of Free Energy Curves

Since geometric phase transitions are first order phase transitions, we can find the set of conditions at which they occur by looking at the first derivative of the free energy with respect to the thermodynamic variables. To do so, we first have to calculate the free energy as a function of the magnetization $F(m)$. The Landau free energy is given by

$$F(m) = -k_{\mathrm{B}}T \ln(p(m)) + F_0, \tag{3.1}$$

where $p(m)$ is the probability of finding the system at magnetization m and F_0 is added to indicate that the free energy is only defined up to an additive constant. In principle with the help of our Monte-Carlo algorithm we could calculate a histogram $H(m_{\mathrm{i}})$ of the magnetization values as they appear in our simulation and since

$$p(m) = \frac{H(m_{\mathrm{i}})}{\sum_i H(m_{\mathrm{i}})} \tag{3.2}$$

the free energy $F(m)$ can be calculated using

$$F(m) = -k_{\mathrm{B}}T \ln(H(m)) \tag{3.3}$$

where the additive constant has been omitted.
However in the Ising model below the critical temperature, $F(m)$ is characterized by two minima corresponding to the predominantly spin-up and spin-down configurations respectively which are separated by a free energy barrier. In a simple Metropolis Monte Carlo simulation of such a system, we find the situation shown in figure 3.1. The magnetization of the system stays around the two equilibrium values and we hardly if ever see transitions between those two regimes. Hence for the magnetization values in between we will achieve only bad statistics if we are able to calculate anything at all. To overcome these limitations a *multiple histogram* method was used which will be described in the next section.
The methods described here can later also be used to calculate free energies as functions of arbitrary other order parameters.

3.1. Self Consistent Histograms

3.1.1. The Basic Concept

The self consistent histogram method has first been introduced by Ferrenberg and Swendsen [14]. The description given here follows the one by Frenkel and Smit [2].

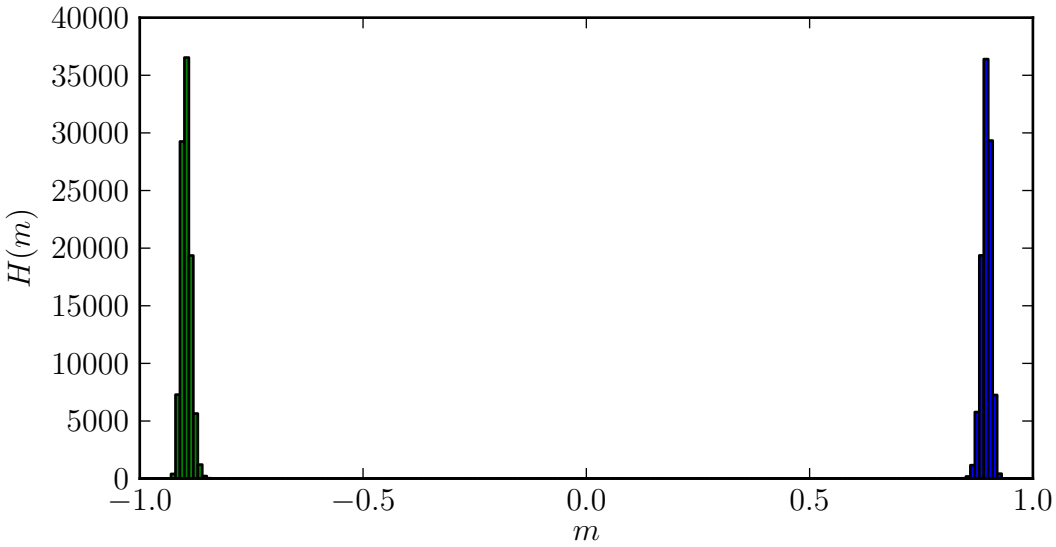

Figure 3.1.: Histogram of magnetization values encountered in two separate Metropolis Monte-Carlo simulations of the square lattice Ising model with 100×100 spins at a temperature of $0.9\ T_C$. 10^6 passes have been performed in each simulation starting from a previously equilibrated starting configuration. Notice that the values in between the two equilibrium magnetizations have never been observed and hence the free energy landscape in this region can not be estimated from these calculations.

We look at a set of Hamiltonians $\mathcal{H}_j$ that are defined by

$$\mathcal{H}_j = \mathcal{H} + W_j(Q[\sigma]), \tag{3.4}$$

where $Q(\sigma)$ is some order parameter calculated from the state of the system σ. For each Hamiltonian we can write down the associated canonical probability distribution of the order parameter Q

$$p_j(Q) = \frac{\int \mathrm{d}\sigma\ e^{-\beta(\mathcal{H}+W_j(Q[\sigma]))}\ \delta[Q - Q[\sigma]]}{\int \mathrm{d}\sigma\ e^{-\beta(\mathcal{H}+W_j(Q(\sigma]))}}, \tag{3.5}$$

where $\int \mathrm{d}\sigma$ denotes an integral over all states. In the case of the Ising model the numerator reduces to a discrete sum over all configurations which satisfy $Q(\{\sigma_i\}) = Q$ and the denominator is a sum over all configurations. The denominator defines the canonical partition function Z_j associated with $\mathcal{H}_j$

$$Z_j = \int \mathrm{d}\sigma\ e^{-\beta(\mathcal{H}+W_j(Q(\sigma]))}. \tag{3.6}$$

In principle we can calculate the probability distribution associated with the original Hamiltonian $\mathcal{H}$

$$p_0(Q) = \frac{1}{Z_0} \int \mathrm{d}\sigma\ e^{-\beta\mathcal{H}}\ \delta[Q - Q[\sigma]] \tag{3.7}$$

from each one of the distributions p_j. This can be seen by calculating the ratio p_0/p_j:

$$\frac{p_0(Q)}{p_j(Q)} = \frac{Z_j}{Z_0} \frac{\int \mathrm{d}\sigma\, e^{-\beta\mathcal{H}}\, \delta[Q - Q[\sigma]]}{\int \mathrm{d}\sigma\, e^{-\beta(\mathcal{H}+W_j(Q([\sigma]))}\, \delta[Q - Q[\sigma]]} = e^{\beta W_j(Q)} \frac{Z_j}{Z_0}, \tag{3.8}$$

where we have used that with the help of the δ function in the integral we can pull out a factor of $e^{\beta W_j}$ from the denominator. In practice, however, the histograms gathered may not overlap or suffer from bad statistics where they do and we want to calculate the ratio Z_j/Z_0 using data from the windows in between. To do so one chooses the ansatz

$$p_0(Q) = \sum_{\mathrm{j}=1}^{n} w_j(Q)\, e^{\beta W_j} \frac{Z_j}{Z_0} p_j(Q) \tag{3.9}$$

with

$$\sum_j w_j(Q) = 1. \tag{3.10}$$

We want to choose the coefficients w_j such that the variation of our estimate is minimized. Using that the simulations within different windows are not correlated and therefore $\left\langle p_j(Q) p_k(Q) \right\rangle = \left\langle p_j(Q) \right\rangle \left\langle p_k(Q) \right\rangle$, we can write

$$\begin{aligned}
&\left\langle p_0(Q)^2 \right\rangle - \left\langle p_0(Q) \right\rangle^2 \\
&\quad = \left\langle \left(\sum_j w_j(Q)\, e^{\beta W_j} \frac{Z_j}{Z_0} p_j(Q) \right)^2 \right\rangle - \left\langle \sum_j w_j(Q)\, e^{\beta W_j} \frac{Z_j}{Z_0} p_j(Q) \right\rangle^2 \\
&\quad = \sum_{j,k} w_j(Q) w_k(Q) e^{\beta(W_j+W_k)} \frac{Z_j Z_k}{Z_0^2} \left\langle p_j(Q) p_k(Q) \right\rangle \\
&\qquad - \sum_{j,k} w_j(Q) w_k(Q) e^{\beta(W_j+W_k)} \frac{Z_j Z_k}{Z_0^2} \left\langle p_j(Q) \right\rangle \left\langle p_k(Q) \right\rangle \\
&\quad = \sum_j w_j(Q)^2\, e^{2\beta W_j} \frac{Z_j^2}{Z_0^2} \left(\left\langle p_j(Q)^2 \right\rangle - \left\langle p_j(Q) \right\rangle^2 \right)
\end{aligned}$$

We use our normalized histogram counts $H_j(Q)/N_j$ as estimates for $p_j(Q)$ and assume that they are Poisson-distributed, meaning that

$$\left\langle p_j(Q)^2 \right\rangle - \left\langle p_j(Q) \right\rangle^2 = \frac{\left\langle H_j(Q)^2 \right\rangle - \left\langle H_j(Q) \right\rangle^2}{N_j^2} = \frac{\left\langle H_j(Q) \right\rangle}{N_j^2}. \tag{3.11}$$

Now assuming a bin width of ΔQ and together with (3.8) we can write

$$\left\langle p_j(Q)^2 \right\rangle - \left\langle p_j(Q) \right\rangle^2 = \frac{N_j p_j(Q) \Delta Q}{N_j^2} = e^{-\beta W_j(Q)} \frac{Z_0}{Z_j} \frac{p_0(Q) \Delta Q}{N_j}$$

and inserting above yields

$$\left\langle p_0(Q)^2 \right\rangle - \left\langle p_0(Q) \right\rangle^2 = p_0(Q) \sum_j w_j(Q)^2 \, e^{\beta W_j} \frac{Z_j}{Z_0} \frac{\Delta Q}{N_j}. \tag{3.12}$$

To minimize this expression with respect to w_j and under constraint (3.10) we use a Lagrange multiplier α and look at the function

$$f(\{w_j\}, \alpha) = p_0(Q) \sum_j w_j(Q)^2 \, e^{\beta W_j} \frac{Z_j}{Z_0} \frac{\Delta Q}{N_j} - \alpha \left(\sum_j w_j(Q) - 1 \right). \tag{3.13}$$

Setting the partial differential w.r.t. w_j to 0 and absorbing a constant factor of $1/(2p_0)$ into α' gives us

$$w_j(Q) = \alpha' e^{-\beta W_j(Q)} \frac{Z_0 N_j}{Z_j \Delta Q}$$

Using the normalization (3.10) to determine α' and together with our initial ansatz (3.9) we arrive at an expression for our estimate p_0

$$p_0(Q) = \frac{\sum_j \frac{N_j p_j(Q)}{\Delta Q}}{\sum_k e^{-\beta W_k(Q)} \frac{N_k Z_0}{Z_k \Delta Q}} = \frac{\sum_j H_j(Q)/\Delta Q}{\sum_k e^{-\beta W_k(Q)} Z_0 N_k / Z_k}. \tag{3.14}$$

To determine the values Z_j we insert this expression together with (3.8) into (3.6) which yields

$$Z_i = \int \mathrm{d}Q \, e^{-\beta W_i(Q)} \frac{\sum_j H_j/\Delta Q}{\sum_k e^{-\beta W_k(Q)} N_k / Z_k}, \tag{3.15}$$

which is a system of non-linear equations for the Z_is. Having solved these equations, the probability density is calculated using (3.14).

3.1.2. Specialization to Hard Windows

In practice a multiple histogram simulation with hard windows has been used. This means that the order parameter range of interest is divided into a set of overlapping windows and within each window a (for the time) separate simulation is done. The basic Monte-Carlo algorithm is modified by not allowing moves outside of the boundaries of the respective window, which can be formally described by setting the bias potential for window j to

$$W_j = \begin{cases} 0 & \text{for } Q_\mathrm{j}^{(\mathrm{l})} \leq Q(\{\sigma_i\}) \leq Q_\mathrm{j}^{(\mathrm{u})} \\ \infty & \text{otherwise} \end{cases} \tag{3.16}$$

where $Q_\mathrm{j}^{(\mathrm{l})}$ and $Q_\mathrm{j}^{(\mathrm{u})}$ are lower and upper boundary of the window, respectively. As with the simple Monte-Carlo simulations, it is important here to also count the rejected moves when doing statistics in order to obtain correct results. Now looking at expression (3.15) we see that the factor $e^{-\beta W_j}$ suppresses contributions to the integral from Q values outside

the window and that similarly the sum in the denominator is reduced to a sum over the windows k that overlap with the current Q value. Hence we can write

$$Z_i = \int_{Q_i^{(\mathrm{l})}}^{Q_i^{(\mathrm{u})}} \mathrm{d}Q \frac{\sum_j H_j(Q)/\Delta Q}{\sum\limits_{\substack{k \\ Q_k^{(\mathrm{l})} \le Q \le Q_k^{(\mathrm{u})}}} N_k/Z_k}. \tag{3.17}$$

In principle this set of equations can be solved numerically, however if we furthermore assume that only neighboring windows overlap we can deduce a recursive formula. In this case the integral can be split into three contributions as follows:

$$\begin{aligned} Z_i &= \int_{Q_i^{(\mathrm{l})}}^{Q_{i-1}^{(\mathrm{u})}} \mathrm{d}Q \frac{(H_{i-1}+H_i)/\Delta Q}{N_{i-1}/Z_{i-1} + N_i/Z_i} + \int_{Q_{i-1}^{(\mathrm{u})}}^{Q_{i+1}^{(\mathrm{l})}} \mathrm{d}Q \frac{H_i/\Delta Q}{N_i/Z_i} + \int_{Q_{i+1}^{(\mathrm{l})}}^{Q_i^{(\mathrm{u})}} \mathrm{d}Q \frac{(H_i+H_{i+1})/\Delta Q}{N_i/Z_i + N_{i+1}/Z_{i+1}} \\ &= \frac{Z_{-1}Z_i}{N_{i-1}Z_i + N_iZ_{i-1}} \int_{Q_i^{(\mathrm{l})}}^{Q_{i-1}^{(\mathrm{u})}} \mathrm{d}Q \frac{H_{i-1}+H_i}{\Delta Q} + \frac{Z_i}{N_i} \int_{Q_{i-1}^{(\mathrm{u})}}^{Q_{i+1}^{(\mathrm{l})}} \mathrm{d}Q \frac{H_i}{\Delta Q} + \frac{Z_iZ_{i+1}}{N_iZ_{i+1} + N_{i+1}Z_i} \int_{Q_{i+1}^{(\mathrm{l})}}^{Q_i^{(\mathrm{u})}} \mathrm{d}Q \frac{H_i+H_{i+1}}{\Delta Q} \\ &= \frac{Z_{-1}Z_i}{N_{i-1}Z_i + N_iZ_{i-1}} A_i + \frac{Z_i}{N_i} B_i + \frac{Z_iZ_{i+1}}{N_iZ_{i+1} + N_{i+1}Z_i} C_i. \end{aligned}$$

Here the integrals have been abbreviated using A_i,B_i and C_i and the Q dependence of the H_is has been omitted.

3.2. Application to the Ising Model

Throughout this work reweighting has been done using equation(3.14), which is solved using a fixpoint iteration scheme. The integration is carried out using a simple direct summation of the data points. The code and program that performs this calculation has kindly been provided by Philipp Geiger.

To locate the magnetizations at which the geometric phase transitions occur at a temperature of 0.9 T_C free energy calculations using hard windows have been performed. The windows have been chosen such that only neighboring windows overlap and also such that the neighboring histograms show a sufficient overlap with each other. Figure 3.2 shows a collection of histograms gathered and in figure 3.2b they have been reweighted as described previously. Notice that we have only simulated positive magnetizations since the Ising model is symmetric with respect to a magnetization change by a factor (-1).

The dimensionless Landau free energy of the system as a function of m, $F(m)$ is then obtained by taking the negative logarithm of the reweighted histogram. To locate the geometric phase transitions we also look at the derivative of $F(m)$ (figure 3.3b).

It has to be noted however, that if we want to accurately locate geometric phase transitions by this method, we rely upon the simulation to be ergodic. At the given temperature that

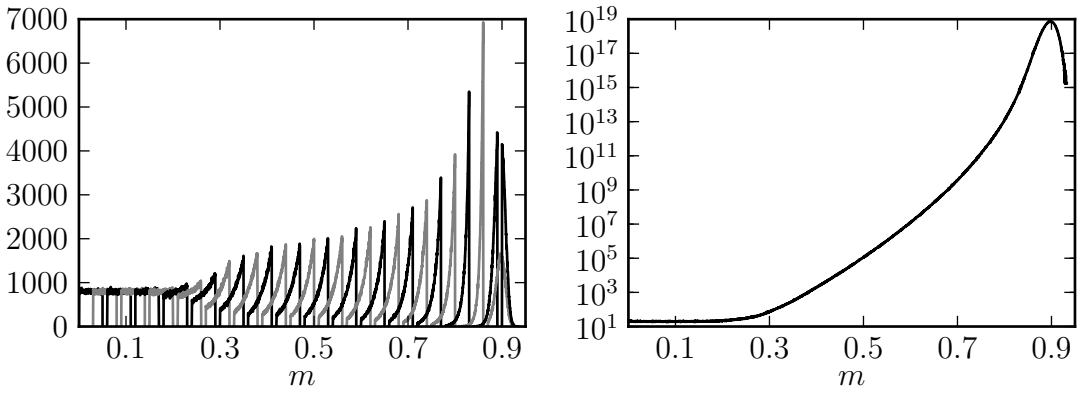

(a) (b)

Figure 3.2.: Histograms obtained using umbrella sampling at a temperature of 0.9 T_C with hard magnetization windows for a 100×100 Ising system. (a) shows the individual histograms obtained and (b) the reweighted histogram, each of them as a function of magnetization m.

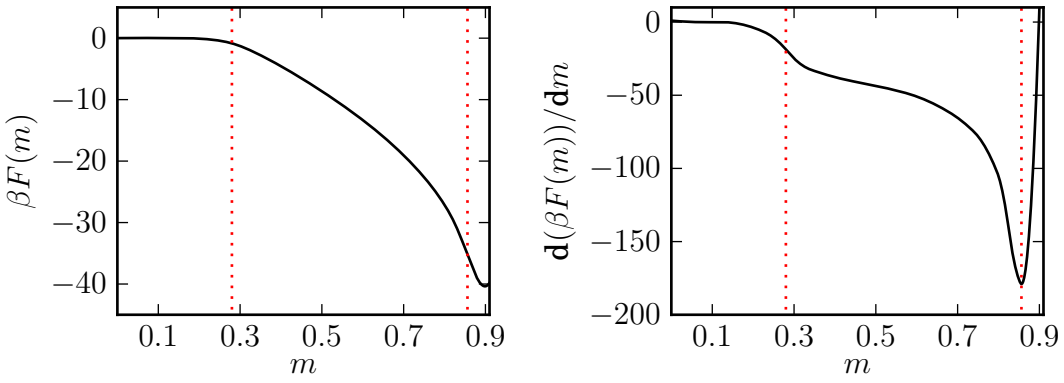

(a) (b)

Figure 3.3.: Dimensionless free energy as a function of magnetization m (a) and its derivative (b) for a 100×100 Ising Model system at a temperature of 0.9 T_C. The free energy has been smoothed using a cubic spline. The dotted lines roughly indicate the magnetizations at which neighboring geometric phases coexist (slab-sphere: ≈ 0.28, homogeneous-cluster: ≈ 0.86).

is rather close to the critical temperature this is given as evidenced by figure 3.4 which shows the order parameter D (see section 5.3.4) as a function of simulation time for a selection of windows close to the slab-sphere transition. We can see that the simulations frequently pass from one side of the transition to the other and, if we assume that the slab-sphere free energy barrier is the only relevant barrier, can conclude that the simulation is ergodic and the relative weights of each of the phases is accurate. Indeed when we look at simulations at constant magnetization of 0.28 at temperature 0.9 T_C these weights turn out to be roughly equal (see figure 5.18).

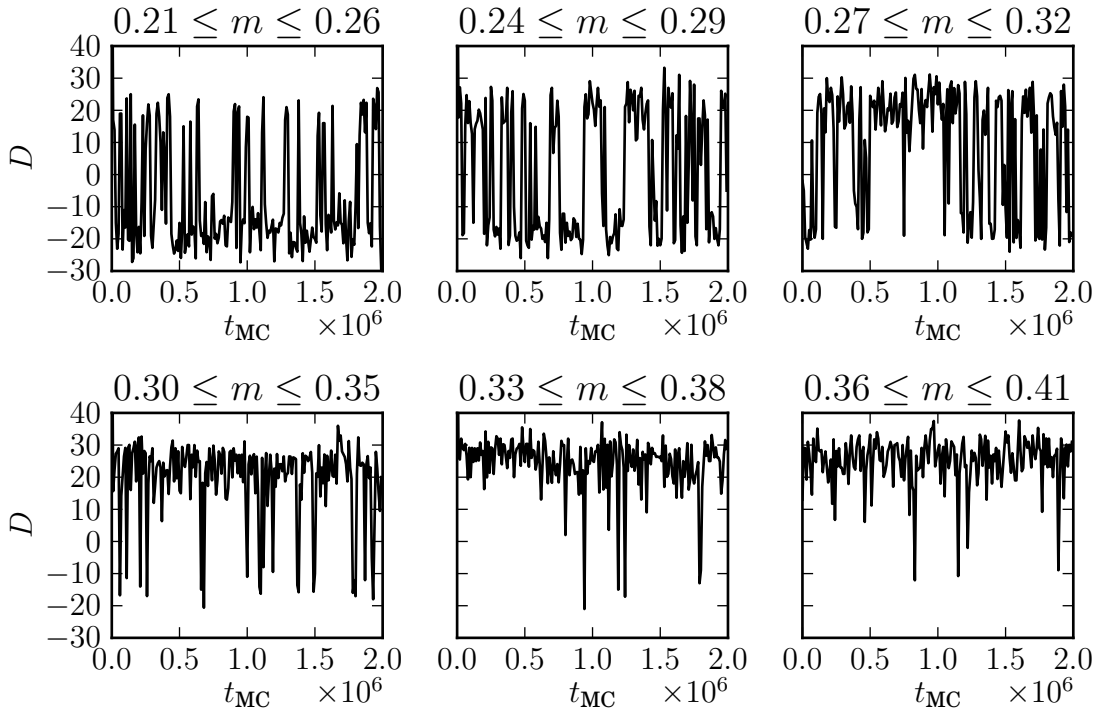

Figure 3.4.: Order parameter D (see section 5.3.4) as a function of simulation time for a set of simulations in the 100×100 Ising model at temperature 0.9 T_C constrained to the magnetizations shown above each diagram. The magnetization windows are chosen to be around the slab-sphere phase transition that occurs around a magnetization of 0.28. Positive values of D signify spherical and negative values slab like configurations.

In the case of the 2D Ising model the slab-sphere transition turns out to be the limiting factor in this type of calculations, since the free energy barrier between slab- and spherical configurations is much larger than the one for the nucleation process at the homogeneous-cluster transition. In fact even for slightly lower temperatures the simulations around the slab-sphere transition become stuck in one of the two phases as shown in 3.5 and hence the free energy curve obtained is not reliable anymore.
The size of the system is limited by a similar problem. As we shall see in section 5.3.2 the

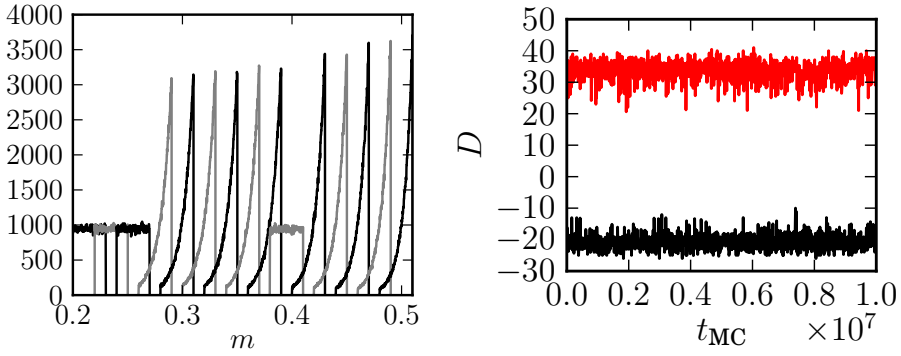

(a) (b)

Figure 3.5.: (a) Umbrella sampling histograms for a selection of magnetization windows around the sphere-slab transition at temperature 0.7 T_C. One can clearly see a window that is atypically stuck in a slab-like configuration, indicating a breakdown of ergodicity. (b) Order parameter D as a function of simulation time for a simulation constrained to magnetizations $0.38 \leq m \leq 0.41$ (black) and $0.40 \leq m \leq 0.43$ (red). Positive values of D signify spherical and negative values slab like configurations. It can be seen that in the course of the simulation transitions between the two phases never occur and hence the resulting estimate of the free energy is necessarily inaccurate.

height of the energy barrier that separates slab from spherical configurations is proportional to the linear size of the system. Even for a slightly larger system than the one of size 100×100 shown here, the umbrella sampling run takes a long time to converge or does not converge at all.

To overcome these difficulties one has to use more advanced methods such as parallel tempering or other methods such as Wang-Landau simulations. To locate the phase transitions at lower temperatures we will rely upon calculations performed by Andreas Tröster using the Wang-Landau algorithm.

4. Reaction Coordinates - Concepts

In studying a phase transition, we first have to be able to identify whether a system is in one or the other state. A quantity that accomplishes this task is called an *order parameter*.

As a second step we want to understand what the key factors are that play a role in the transition. An important ingredient for such a study is what is known as a *reaction coordinate*, a single number that specifies how far a transition has already proceeded [15]. In the following we will establish how to assess the quality of a given reaction coordinate which we will then use in section 5 to tackle the problem of geometric phase transitions.

4.1. The Commitor Distribution

We can construct an infinite number of coordinates when we try to describe how a phase transition proceeds. However, having an order parameter does not automatically imply that it also provides us with the right picture of how the phase transition occurs (see Bolhuis et al. [16] for examples of what can go wrong).

To decide whether a coordinate $Q(\{\sigma\})$ is a "good coordinate" in the sense that it provides physical insight let us introduce the *commitor distribution* (the following description follows the one given by Tuckerman [17]). Consider the situation outlined in figure 4.1: Within the set of possible configurations $\{\sigma_i\}$, we can identify the two (disjoint) sets of configurations $\mathcal{A}$ and $\mathcal{B}$ which contain configurations in the two phases of interest[1]. For each configuration that is not a member of either of those sets, we can define the *commitor probability* $P_{\mathcal{B}}(\{\sigma_\mathrm{i}\})$ as the probability that a trajectory started at configuration $\{\sigma_\mathrm{i}\}$ reaches region $\mathcal{B}$ first. The commitor is considered to be the ideal reaction coordinate [15, 18], however its calculation is costly and does by itself not provide physical insight, which is why we try to find a reaction coordinate that reproduces the isosurfaces of the commitor distribution [15].

In our search for a good reaction coordinate we proceed by studying the commitor $P_{\mathcal{B}}(Q)$, calculated in constant magnetization simulations, for each proposed coordinate $Q(\{\sigma_\mathrm{i}\})$, to see whether there is a clear relationship visible (i.e. $P_{\mathcal{B}}$ is well described by some monotonic function $f(Q)$). When we have found a suitable candidate coordinate, we further quantify the quality of it by looking at the *transition states*, which are states that are expected to have a commitor probability $P_{\mathcal{B}}$ of $1/2$, using a procedure called a histogram test.

[1] We assume here that there are no other (meta-)stable states

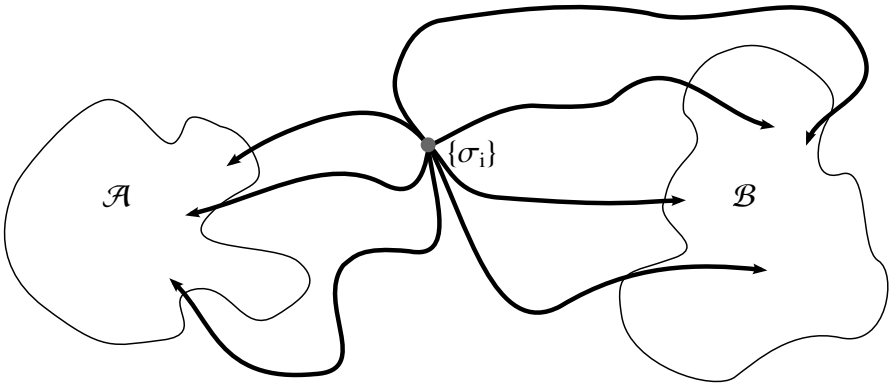

Figure 4.1.: Schematic representation of the procedure used to define and calculate commitor probabilities.

4.2. The Histogram Test

After having found a candidate for a reaction coordinate, we can determine the value Q^* for which we expect the commitor probability to be $1/2$. The set of all states $\{\sigma\}$ that fulfill $Q(\{\sigma\}) = Q^*$ represent a trial transition state surface. If our reaction coordinate works well, this trial surface closely resembles the transition state surface of our system, i.e. the surface with $P_{\mathcal{B}} = 1/2$, and hence if we calculate the commitors for states on this trial surface we expect to get a distribution of probabilities $h(p)$ that is sharply peaked around $1/2$ [16, 18].

Since we can only estimate commitor probabilities using a finite number of trajectories our estimates will naturally contain noise. If the trial transition state surface would exactly reproduce the true transition state surface, we would expect $h(p)$ to be a binomial distribution. Any deviation, however, will result in an excess variance observed. Setting the mean of $h(p)$ to be μ_h, the root mean square difference σ of the trial surface to the transition state surface can be estimated using [19]

$$\sigma^2 = \frac{N}{N-1}\left(\sigma_h^2 - \frac{1}{N}\mu_h(1-\mu_h)\right), \tag{4.1}$$

where σ_h^2 may take values between $\mu_h(1-\mu_h)/N$ and $\mu_h(1-\mu_h)$ corresponding to a perfect reproduction of the isocommitor surface and to a mixture of states from $\mathcal{A}$ and $\mathcal{B}$ respectively. Hence σ^2 may vary from 0 to $\mu_h(1-\mu_h) = \sigma_h$.

The estimated probability of the surface chosen by the coordinate is simply estimated to be

$$\mu = \mu_h. \tag{4.2}$$

For sufficiently narrow intrinsic commitor distributions and values of μ close enough to $1/2$ the uncertainties can also be estimated [19]. If nN is the total number of trajectories

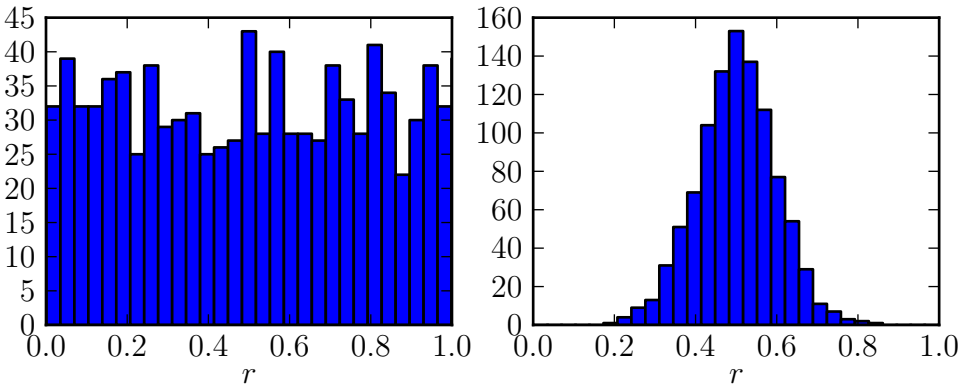

Figure 4.2.: Examples of histogram tests performed on sequences of outcomes that were chosen using random number generators. For each data point the probability of outcome $\mathcal{B}$ is chosen, a set of outcomes is randomly generated using this probability and then the probability is estimated over all of these outcomes. On the left a bad reaction coordinate that does not resemble the true commitor and hence outcomes were chosen with random probabilities. This sample yields $\mu = 0.501 \pm 0.005$ and $\sigma = 0.294 \pm 0.007$. On the right a perfect reaction coordinate which means that the probability of outcome $\mathcal{B}$ is $1/2$ and therefore the histogram test yields a sample from a binomial distribution with probability $1/2$ ($\mu = 0.501 \pm 0.002$, $\sigma = 0.025 \pm 0.008$). For each histogram 1000 sequences of 30 random choices each have been generated.

used they equate to:

$$\frac{\delta\mu}{\mu} = \sqrt{\frac{0.25 + (N-1)\sigma^2}{Nn}} \tag{4.3}$$

$$\frac{\delta\sigma}{\sigma} = \frac{1}{2\sqrt{(N-1)Nn}} \left(\frac{1}{8\sigma^4} + \frac{N-2}{\sigma^2} + 2\left((N-3)^2 - N\right) \right)^{1/2} \tag{4.4}$$

4.3. Maximum Likelihood Approaches to finding Reaction Coordinates

Although for some systems it is possible to find a single reaction coordinate that describes a phase transition well [20], in other systems multiple influences that determine the commitor probability have been identified. In particular, for nucleation in the Ising model Pan and Chandler [21] have shown that critical nuclei are not only characterized by the size of the largest cluster in the system, but also by its surface and other variables.
Peters et al. [15, 19, 22] have presented a scheme that combines multiple coordinates to form a single reaction coordinate in an optimal way using a likelihood maximization scheme. They model the commitor probability $P_{\mathcal{B}}$ as a sigmoid function of a combined

coordinate r, for example

$$P_{\mathcal{B}}(r) = \frac{1}{2}(1 + \tanh(r)). \tag{4.5}$$

In the simplest case the candidate collective variables $Q_i(\{\sigma\})$ are combined via a linear combination

$$r = \alpha_0 + \sum_i \alpha_i Q_i(\{\sigma\}) = \alpha_0 + \boldsymbol{\alpha} \cdot \boldsymbol{Q}(\{\sigma\}), \tag{4.6}$$

where the α_i and Q_i have been gathered in the vectors $\boldsymbol{\alpha}$ and $\boldsymbol{Q}$ but one may also introduce higher order terms or even a quadratic form $\boldsymbol{Q}^T \boldsymbol{A}\boldsymbol{Q}$ to incorporate interactions between the variables [15].
Given a set of trajectories starting at initial configurations $\{\sigma_i\}$ which commit exclusively to either region $\mathcal{A}$ or $\mathcal{B}$ we can now define the likelihood of our model to be

$$L = \prod_{\{\sigma_i\}\to\mathcal{A}} [1 - P_{\mathcal{B}}(r(\{\sigma_i\}))] \prod_{\{\sigma_i\}\to\mathcal{B}} P_{\mathcal{B}}(r(\{\sigma_i\})) \tag{4.7}$$

where $\prod_{\{\sigma_i\}\to\mathcal{A}}$ denotes a product over all trajectories that commit to region $\mathcal{A}$ and similarly for region $\mathcal{B}$. The dynamics of the Ising model depend on a sequence of random numbers which makes it a diffusive model and hence justifies using a likelihood of this form and also that we can use all trajectories started from a single configuration since they are independant realizations of $P_{\mathcal{B}}$ [15].
For numerical reasons the log-likelihood $\log(L)$ is then maximized over the coefficients α_i and $A_{i,j}$ where applicable.
Using this method we can test, even in an automatic fashion, various combinations of coordinates using only a single set of trajectories. One has to be careful however, since adding model complexity will always allow us to improve the likelihood. Peters et al. consider the improvement in likelihood to be significant if it is greater than the quantity $(1/2)\ln(N)$ where N is the total number of trajectories [15][2]. Additionally we check the quality of the obtained coordinate using a verification set of configurations and by performing a histogram test.
The above algorithm has been implemented by Clarion Tung using a BFGS method which has kindly been provided to me.

[2]This criterion can be inferred from Bayesian statistics.

5. Reaction Coordinates - Application to Geometric Transitions

5.1. Cluster Calculation

For the purpose of this work, we will use a geometrical definition of clusters of equally oriented spins. Two spins belong to the same cluster, if they are neighbors of each other and have the same orientation [21]. Suppose that we look for clusters that are made up of spins with orientation -1 then the algorithm employed looks like this:

1. Pick a random first spin with orientation -1 from the configuration that has not yet been considered.
2. We set up a data structure, called the frontier, that initially contains the spin we have chosen in step 1.
3. Take a spin from the frontier, meaning that it is at the same time removed, and look at each of its four neighbors. Pick those that have the same orientation and that have not previously been added to the frontier and add them to the frontier.
4. Add the spin to our cluster.
5. As long as the frontier is not empty, repeat points 3 and 4 to find all spins that are part of this cluster.
6. If there are still unvisited spins with orientation -1 start again at step 1 and construct the next cluster. If we are only interested in the largest cluster, we may stop when there are not enough spins left to form an even larger cluster than the ones already found.

In the worst case scenario, the largest cluster in the system is the one we find last, which means we have to look at each spin of the configuration that has orientation -1. This gives rise to order N steps of type 3, where N is the size of the system. Step 3 involves five lookups within the frontier and four lookups within the configuration which can all be carried out in constant time. Hence the worst case running time of the procedure is proportional to N.
This algorithm gives us clusters of spins, which may or may not span over box boundaries. However to calculate quantities like the “center of mass” of a cluster, we need to reconstruct the shape of the cluster as it would be, if no periodic boundary conditions had been applied (see fig. 5.1 for an example).
This reconstruction can be done by amending step 4 in the procedure above:

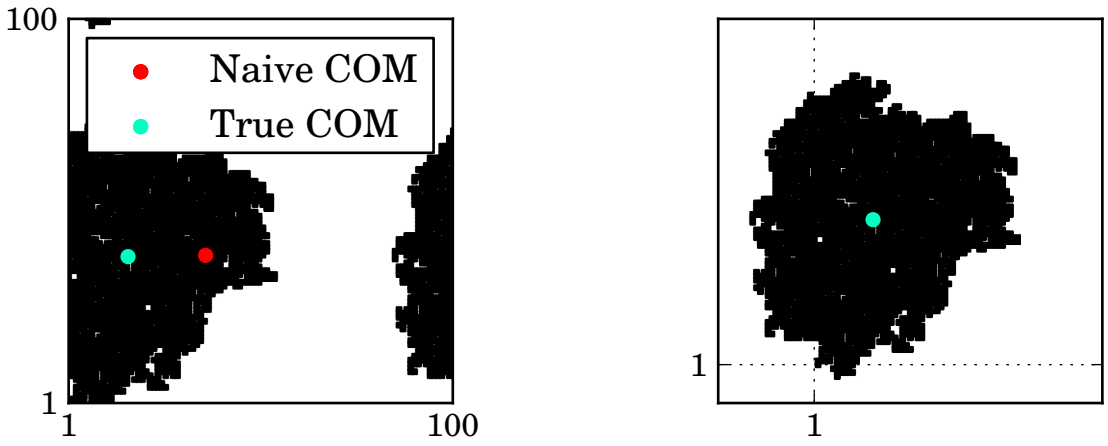

Figure 5.1.: Example of a typical cluster found in the simulation. On the left the cluster is shown with periodic boundary conditions applied. On the right hand side the shape of the cluster has been reconstructed (the boundaries of the simulation box are indicated by dotted lines). To demonstrate the need to reconstruct a clusters shape as it would be if there were no periodic boundary conditions, the center of mass (COM) has been calculated naively and by using the reconstructed cluster on the right.

4'. Add the spin to the cluster and note its position in the simulation box as well as its absolute position relative to the starting spin (or some other reference point). This absolute position is calculated by incrementing the absolute position of the spin from which this spin has been constructed (i.e. if the spin is to the right of the spin it was constructed from, add $+1$ to the x coordinate, if the spin is below add -1 to the y coordinate, and so on).

If the cluster does not span the simulation box, this algorithm yields unique results up to a translation of the cluster. However care has to be taken if the cluster spans the simulation box, in which case the shape of the reconstructed cluster depends on the details of the algorithm, such as the starting spin and the sequence in which numbers are added to and removed from the frontier.

Particularly peculiar results can be obtained by exploring the cluster in a depth first search manner, meaning that the last point added to the frontier is also the one that is explored next. In some cases this will yield a cluster that is drawn out like a string and spans multiple boxes in one direction. If a breadth first strategy is chosen (i.e. points are explored upon in the sequence they were added to the frontier), this error of spanning multiple boxes is avoided, however the details of the reconstructed cluster are still dependant on the factors mentioned above.

An alternative approach to the one described here, is known as the *Hoshen-Kopelmann* [23] algorithm which can be easily parallelized by breaking the simulation box down into subsystems [24] (see Tiggemann [25] for an overview and further references).

5.2. The Evaporation/Condensation Transition

5.2.1. Previous Results

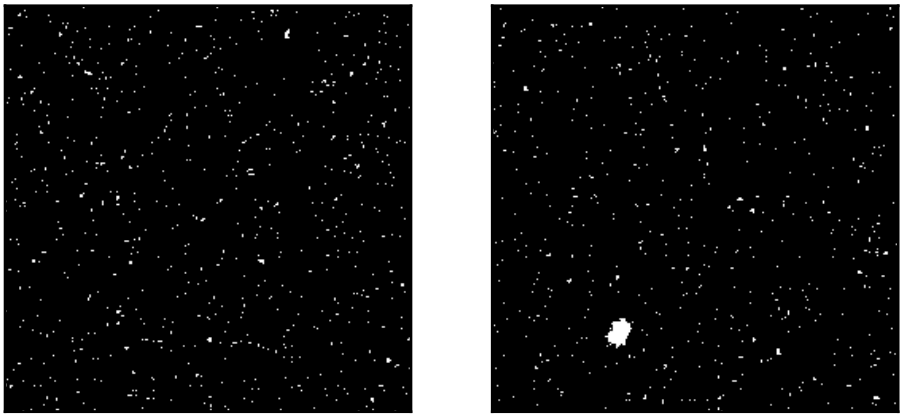

Figure 5.2.: Two example configurations obtained from a simulation of a 256×256 Ising system at fixed magnetization 0.972 and temperature 0.7 T_C. While on the left the spins with value 1 are scattered throughout the system, on the right a large number of them has formed a cluster. In fact the largest cluster in the left configuration contains 13 spins, while in the right configuration the cluster contains 177 spins.

The transition from a system where the spins pointing opposite to the majority direction are distributed homogeneously throughout the system to one where they are (as we shall see) partly grouped together into a larger cluster is referred to in the literature as the Evaporation/Condensation Transition. It has received attention as early as 1965 in a paper by Mayer and Wood [26] who developed a simple model for a 2 dimensional system that already includes geometric phases. We shall develop a similar model in section 5.2.2 and compare it to simulation results.
The ansatz chosen here uses what is known as the capillarity approximation: the surface tension measured for microscopic droplets is assumed to be independent of the curvature of the interface and equal to the one for macroscopic droplets. The particular problem of finding a more realistic description for the radius dependence of the surface tension has spawned recent interest in the evaporation/condensation transition since the droplets forming in finite systems can be used to calculate surface tensions as function of droplet radii from simulation [27–30].
For the transition itself there are some analytic results available by Biskup et al. who have shown that at droplet formation only a fraction of the excess density is used to form a cluster while the rest is absorbed by the surrounding bulk [31]. In particular for the 2D Ising model results in the limit of an infinitely large system can be derived [32] which state that the fraction of the excess magnetization that is absorbed by the droplet λ junps from

0 to $\frac{2}{3}$ at a critical value of the overall magnetization. They do so by assuming a cluster of "Wulff shape" [10, 33, 34] to be in coexistence with the bulk and adjust λ such that the total free energy of the system is minimized. Figure 5.3 shows a plot of their prediction as a function of a rescaled excess magnetization Δ given by

$$\Delta = \frac{2m_0^2 v_L^{3/2}}{\chi N \tau_W}, \tag{5.1}$$

where m_0 is the equilibrium magnetization, χ is the susceptibility, τ_W is the interface free energy per unit volume of the Wulff droplet given by (2.6) and v_L is the equivalent volume of the excess in magnetization given by

$$v_L = \frac{N}{2}(m_0 - m). \tag{5.2}$$

Nußbaumer et al. [35, 36] compared these results to simulation finding them to be in good

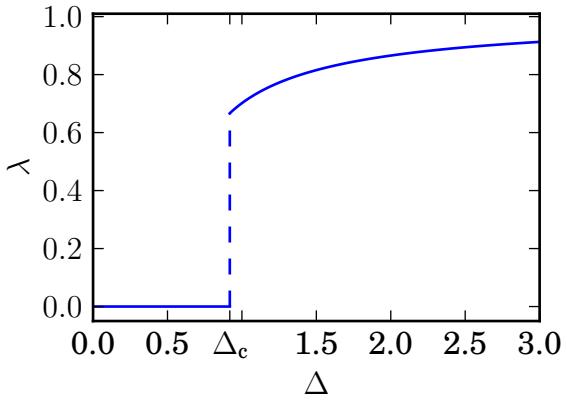

Figure 5.3.: Fraction of total excess magnetization λ that is absorbed by a droplet as function of the rescaled excess magnetization Δ in the 2D Ising model as calculated by Biskup et al. [32]

agreement for large enough lattice sizes. Additionally they examined the height of the free energy barrier at Δ_c using the theory of Biskup et al. which for the Ising model predicts a behaviour according to

$$\beta\Delta F \approx 0.1522 N^{1/3} \tag{5.3}$$

in the infinite volume limit. For large lattice sizes exceeding linear lengths of roughly 150 to 200 spins, the height of the energy barrier at the coexistence magnetization (chosen by requiring the evaporated and condensated phase to have equal weight) exhibits the predicted behaviour.
The dynamics of the nucleation process itself have been studied for the formation of clusters filling the whole system if a magnetic field (or difference in chemical potential if we think of a lattice gas) is applied [15, 21]. Peters and Trout [15] have concluded in their

analysis that one can improve the estimate of commitor probabilities by including the surface of the largest cluster into the calculation. In particular, for a 2D Ising system a larger surface promotes the formation of a cluster. We will treat the formation of equilibrium droplets in a finite system in a similar way in section 5.2.4.

5.2.2. Classical Nucleation Theory

We will apply the concepts of Classical Nucleation Theory (CNT) to the formation of a single spherical cluster in a finite system of volume V at constant mean magnetization m. We denote the volumes of the two domains characterized by opposite prevailing spin direction by V_c and V_b for the cluster and the surrounding bulk and the number of spins with value +1 in each of the domains by N_c and N_b. The mean magnetizations are given by $m_i = 2N_i/V_i - 1$ which have to satisfy the overall magnetization equation

$$m = \frac{V_\mathrm{c} m_\mathrm{c} + (V - V_\mathrm{c}) m_\mathrm{b}}{V} = \alpha_\mathrm{c} m_\mathrm{c} + (1 - \alpha_\mathrm{c}) m_\mathrm{b}, \tag{5.4}$$

where α_c is the fraction of the system that belongs to the cluster. For the free energy of the system we choose the CNT ansatz

$$F(V_\mathrm{c}, m_\mathrm{c}, m_\mathrm{b}) = V_\mathrm{c} f(m_\mathrm{c}) + (V - V_\mathrm{c}) f(m_\mathrm{b}) + S(V_\mathrm{c}) \gamma(V_\mathrm{c}, m_\mathrm{c}, m_\mathrm{b}), \tag{5.5}$$

where $f(m)$ is the free energy per volume of a homogeneous system at magnetization m, S is the surface of the cluster and γ is the interface tension.
Given a fixed volume of the cluster V_c the magnetizations within the two phases will adjust such that $F(m_\mathrm{c}, m_\mathrm{b})$ is minimal. We write

$$\begin{aligned} \frac{\partial F(m_\mathrm{c}, m_\mathrm{b})}{\partial m_\mathrm{c}} &= V_\mathrm{c} \frac{\mathrm{d} f(m_\mathrm{c})}{\mathrm{d} m_\mathrm{c}} + (V - V_\mathrm{c}) \frac{\mathrm{d} f(m_\mathrm{b})}{\mathrm{d} m_\mathrm{c}} + S(V_\mathrm{c}) \frac{\partial \gamma(m_\mathrm{c}, m_\mathrm{b})}{\partial m_\mathrm{c}} \\ &= V_\mathrm{c} \left(\frac{\mathrm{d} f(m_\mathrm{c})}{\mathrm{d} m_\mathrm{c}} - \frac{\mathrm{d} f(m_\mathrm{b})}{\mathrm{d} m_\mathrm{b}} \right) + S(V_\mathrm{c}) \frac{\mathrm{d} \gamma(m_\mathrm{c})}{\mathrm{d} m_\mathrm{c}} \end{aligned} \tag{5.6}$$

where in the second line (5.4) was used. We arrive at the magnetization values at given cluster volume V_c $\hat{m}_\mathrm{c}$ and $\hat{m}_\mathrm{b}$ by approximating $\gamma(m_\mathrm{c})$ to be a constant[1] and setting (5.6) equal to zero:

$$\left. \frac{\mathrm{d} f_\mathrm{c}(m_\mathrm{c})}{\mathrm{d} m_\mathrm{c}} \right|_{m_\mathrm{c} = \hat{m}_\mathrm{c}} = \left. \frac{\mathrm{d} f_\mathrm{b}(m_\mathrm{b})}{\mathrm{d} m_\mathrm{b}} \right|_{m_\mathrm{b} = \hat{m}_\mathrm{b}} \tag{5.7}$$

In order to make a quantitative prediction of the stable states and the energy barrier separating them, we expand the free energy density to second order around the equlibrium magnetizations $\bar{m}_\mathrm{c}$ and $\bar{m}_\mathrm{b}$[2].

$$\begin{aligned} f_\mathrm{c}(m_\mathrm{c}) &= \frac{k_\mathrm{c}}{2} (m_\mathrm{c} - \bar{m}_\mathrm{c})^2 \\ f_\mathrm{b}(m_\mathrm{b}) &= \frac{k_\mathrm{b}}{2} (m_\mathrm{b} - \bar{m}_\mathrm{b})^2 \end{aligned} \tag{5.8}$$

[1] Given the small radii of the clusters formed this assumption is questionable, however in order to test whether the ansatz is able to predict the phase transition we use it here.

[2] Note here that for ease of notation we are writing down two functions here despite the fact that it is actually the same function but defined for different magnetizations.

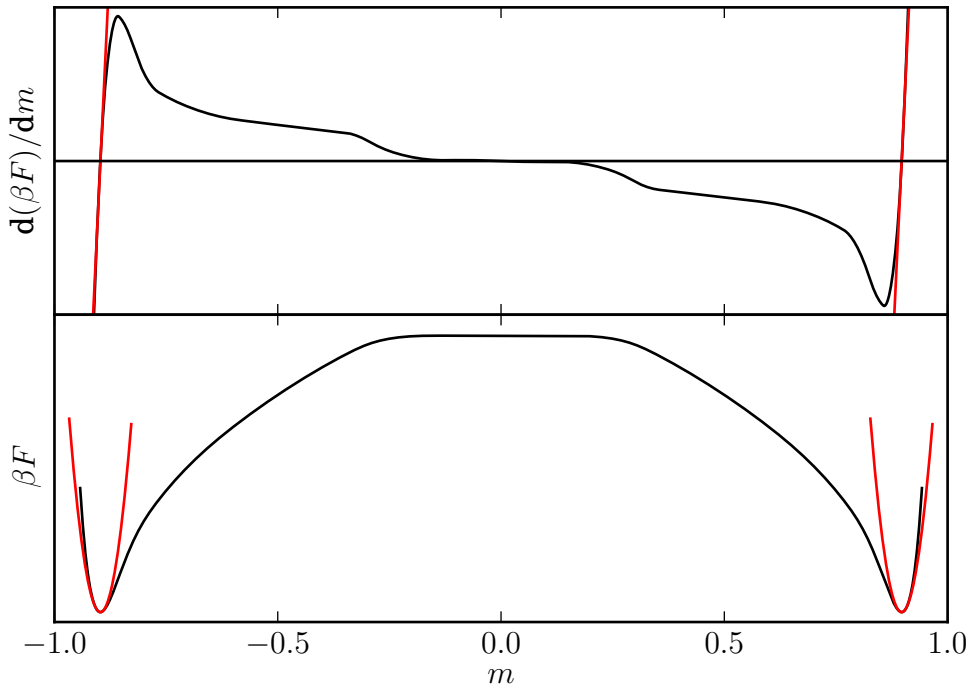

Figure 5.4.: Example free energy as a function of magnetization m for a square lattice Ising Model (lower part) and its derivative (upper part) with respect to m. The red parabolas have been fitted to the free energy around its two minima in order to approximate the free energy of the homogeneous system for magnetizations close to equilibrium magnetizations.

The coefficients k_c and k_b can then be calculated from quilibrium simulations. Since in the Ising model the exact free energy density f is symmetric with respect to a change of the magnetization from m to $-m$ and since our ansatz is even in $(m_b - \hat{m}_b)$ we can set

$$k_c = k_b = k. \tag{5.9}$$

Inserting this and (5.8) into (5.7) yields

$$\hat{m}_c - \bar{m}_c = \hat{m}_b - \bar{m}_b$$

which again using (5.4) can be expressed in terms of the given parameters m and α_c as well as the difference of equilibrium magnetizations $\Delta\bar{m} = \bar{m}_c - \bar{m}_b$[3]:

$$\begin{aligned} \hat{m}_c &= m + (1 - \alpha_c)(\Delta\bar{m}) \\ \hat{m}_b &= m - \alpha_c(\Delta\bar{m}) \end{aligned} \tag{5.10}$$

[3]Note here that $\bar{m}_c$ and $\bar{m}_b$ do not meet (5.4) since they are not measured in coexisting phases whereas $\hat{m}_c$ and $\hat{m}_b$ do.

Unsurprisingly, since we used the same symmetric potential on both sides, the difference of these two magnetizations is exactly $\Delta\bar{m}$ (or equivalently their deviation from the equilibrium value is the same) and therefore the free energy contribution per volume is the same from both phases, namely

$$f_c(\hat{m}_c) = f_b(\hat{m}_b) = \frac{k}{2}\left(m - \bar{m}_c + \Delta\bar{m}(1-\alpha_c)\right)^2 \tag{5.11}$$

and the free energy of the system becomes

$$F(V_c) = \frac{Vk}{2}\left(m - \bar{m}_c + \Delta\bar{m}(1-\alpha_c)\right)^2 + \gamma S(V_c). \tag{5.12}$$

So far we have not assumed a particular shape of the cluster, now however we look at a disk. Substituting the circumference for $S(V_c)$ we get

$$F(V_c) = \frac{Vk}{2}\left(m - \bar{m}_c + \Delta\bar{m}(1-\alpha_c)\right)^2 + 2\gamma\sqrt{\pi V_c}. \tag{5.13}$$

In figure 5.5 we can see that (5.13) reproduces the basic features we expect; with increasing magnetization the minimum that corresponds to forming a cluster vanishes and reducing the surface tension allows for clusters being formed at higher magnetizations. Also the height of the free energy barrier increases with the surface tension.
In order to compare these functions to results obtained from simulations one has to clarify the role that the free energy (5.12) plays.
First we consider that for cluster size $V_c = 0$ we recover our ansatz for the free energy of a homogeneous system at magnetization m. This quantity already includes contributions from small clusters that form as fluctuations in the homogeneous phase. $F(V_c) - F(0)$ can then be interpreted as the work that is necessary to form a cluster V_c that is bigger than the ones already found in the homogeneous phase. In the following we will refer to such a cluster as a significant cluster.
We can define a probability distribution by setting

$$p(V_c) = \frac{1}{Z_V} e^{-\beta F(V_c)} \tag{5.14}$$

where Z_V is a normalization constant. $p(V_c)$ gives the probability of finding a cluster of size V_c in a system if it is the only significant cluster in the system. However, in practice smaller clusters may coexist with larger ones making the estimate only accurate for clusters that are large enough to prevent the formation of clusters of similar size. In particular, if we look at the set of all clusters found in a simulation we expect to underestimate the number of small clusters since we neglect multiple cluster combinations.
As an order parameter for the nucleation phase transition we use the size of the largest cluster found in the system. Again for large enough clusters in the above sense we expect the probability of the largest cluster in the system to be of size V_c to be estimated by (5.14).

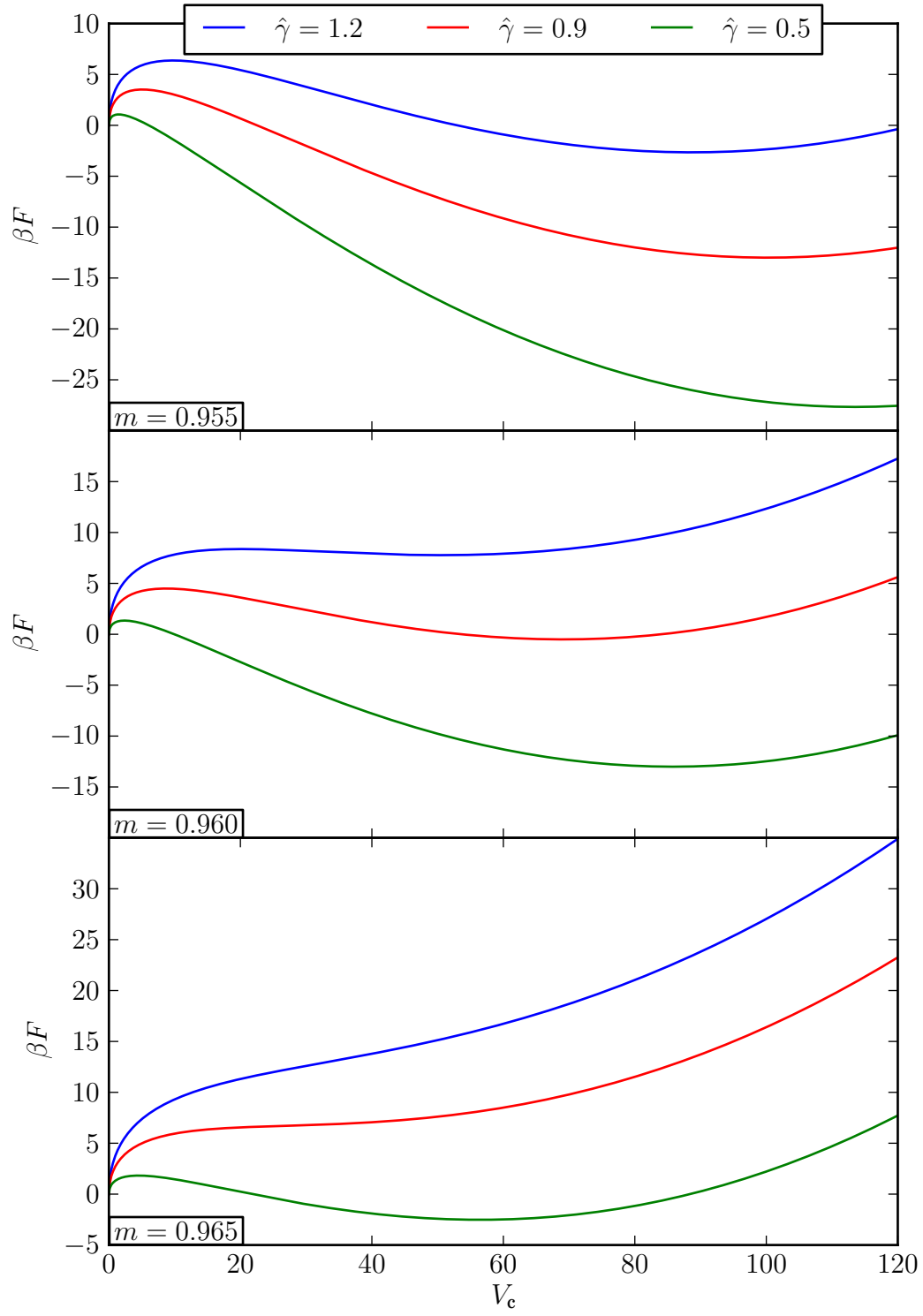

Figure 5.5.: Dimensionless free energy βF as a function of cluster size V_c according to equation (5.13) for the parameters $k = 16$, $\bar{m}_c = -0.9795$, $\Delta\bar{m} = 2\bar{m}_c$. For each magnetization m three different values of the surface free energy $\hat{\gamma} = \beta\gamma$ are shown.

5.2.3. Simulation Results: Comparison to CNT model

The model described in section 5.2.2 contains two parameters which have to be determined from simulations: k and γ.
To determine k an unconstrained MC simulation of the Ising model has been performed and the ansatz (5.8) fitted towards the Landau free energy using k, the mean magnetization $\bar{m}$ and a (physically irrelevant) shift as parameters (figure 5.6).

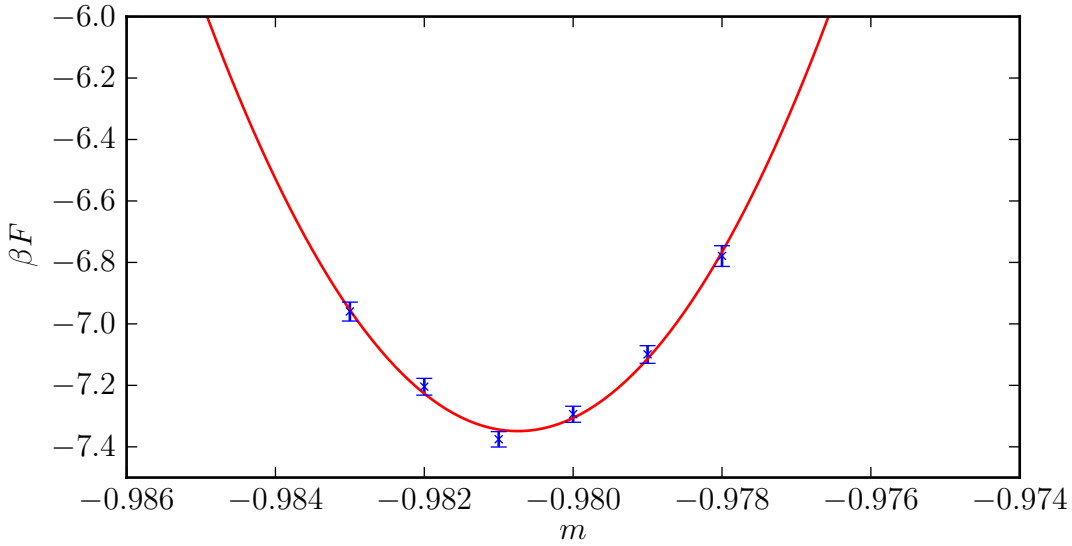

Figure 5.6.: Dimensionless Landau free energy as a function of magnetization m for a 100× 100 Ising system at temperature 0.7 T_c. The results have been obtained using unconstrained Metropolis Monte Carlo method. The blue datapoints show the observed free energies and the associated poissonian uncertainties. The red line shows a fit of the parabolic ansatz (5.8) to the data. The fit yields values of $k = 15.5$ per spin and $\bar{m} = -0.981$.

Determining the surface tension γ is not as straightforward. Canonically one employs what is known as the capillarity approximation [37]. It is the assumption that the surface tension of the curved interface is equal to the one of a planar interface.
We can calculate the latter by noting that the slab configurations we observe around magnetizations of $m = 0$ exhibit two such planar interfaces[4]. The difference in free energy from the homogeneous equilibrium state to the state of $m = 0$ can then be understood as the work necessary to form these two interfaces and hence the planar surface tension per unit length is given by [38]

$$\gamma_\infty = \frac{1}{2L}\left(F(m=0) - F(m=\bar{m})\right) \tag{5.15}$$

[4]These interfaces have been observed to be modulated by capillary waves however these waves are included in the definition of the planar interface [38].

where L is the length of the box.
We use a value of $\gamma_\infty = 0.66$[5] in units of kT per unit length which at a magnetization of 0.961 yields the free energy function shown in figure 5.7 that, although it features a minimum corresponding to the metastable homogeneous region, does not predict the two phases to be at coexistence. Instead one would expect the formation of clusters of a size of roughly 80 spins.

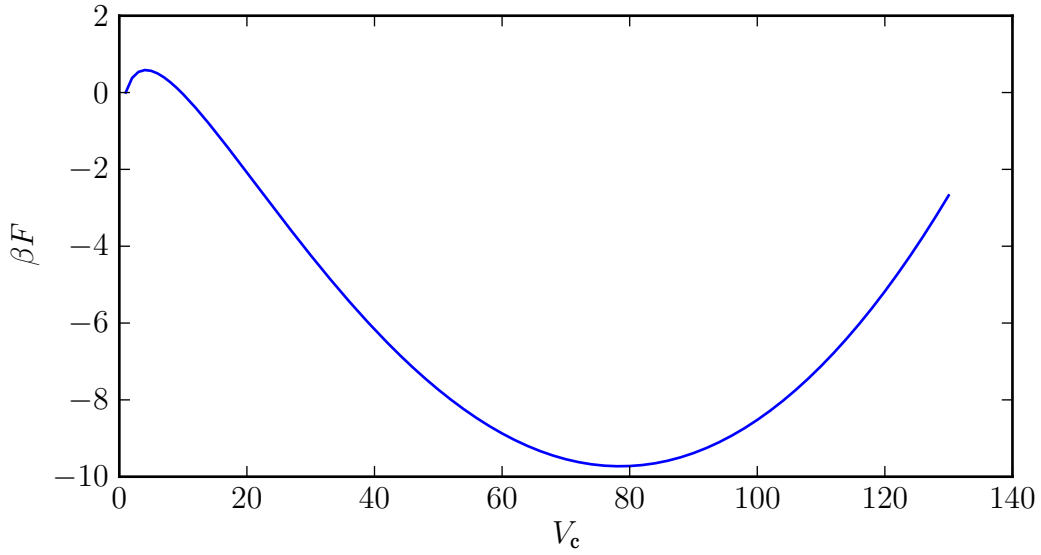

Figure 5.7.: Dimensionless free energy as a function of cluster size predicted by the model (5.13). The parameters $m = 0.961$, $k = 15.5$, $\bar{m} = 0.981$ and the planar interface surface tension $\gamma_\infty = 0.66$ were used.

In principle we would like to find the magnetization at which both phases occur with equal probability in order to predict where the phase transition in the model occurs. This gives us the condition

$$\int_{V_0}^{V_{\max}} \exp(-\beta\, F(V_c)|_{m=m_T})\, \mathrm{d}V_c = \int_{V_{\max}}^{V_1} \exp(-\beta\, F(V_c)|_{m=m_T})\, \mathrm{d}V_c \tag{5.16}$$

where m_T is the phase transition magnetization and we have assumed that the two phases are separated by a maximum in free energy $V_{\max}$. However it turns out that with the planar interface tension measured previously we can not achieve this condition because the maximum in free energy disappears before the two phases have equal weight, making them indisinguishable when looking at the free energy of the system. It should be pointed out here that these calculations are to be taken with a grain of salt since, as was pointed out earlier, the estimates for small cluster sizes are very much doubtful. Taking note of the fact

[5]This value has been obtained from Wang-Landau simulations and is slightly smaller than the analytic estimate using 2.5 at temperature 0.7 T_c that yields a value of 0.675 in units of kT per unit length.

that the probability of finding the system in the cluster phase is reduced with increasing surface tension, one may suspect that the behaviour shown is consistent with an increased surface tension.
To answer this question we take the following approach: we gain an estimate for the surface tension by fitting our model free energy to the one obtained by simulation. However in our CNT model we have implicitly assumed that there is only one significant cluster in the system and hence we first have to find the range of cluster sizes where this assumption is accurate. In figure 5.9 we compare a histogram over the sizes of the largest cluster to a histogram over all clusters found. We can see that the two converge around a cluster size of 50 spins indicating that there can only be one cluster with a size larger than this within the system at the same time[6]. We take this as the lower threshold of the interval over which we carry out the fit. The fit itself is done by minimizing the mean square deviation of the model free energy from the observed free energy as a function of the largest cluster using γ and a shift as parameters. The contributions are weighted proportional to $\sqrt{N}$ where N is the number of datapoints within the respective histogram bin. The result of such a fit is also shown in figure 5.9. We can reproduce the general shape of the histogram for large clusters if we assume a value between 0.8 and 0.9 kT per unit of length for the surface tension. However the exact value obtained using the fit depends somewhat on the interval chosen[7]. In either case it is larger than the planar interface tension.

5.2.4. Simulation Results: The Free Energy Barrier and Reaction Coordinates

CNT in the form described previously makes an implicit assumption: the phase transition can be described using solely the size of the cluster as parameter. In this section we will first investigate this assumption using the methods developed earlier and also use it as a testcase for the maximum likelihood approach.
Since the free energy barrier for the formation of a cluster for a 100×100 system is rather low, we look at a larger system of size 256×256. Figure 5.10 shows the the free energy as a function of the size of the largest cluster for a magnetization of 0.972 and temperature 0.7 T_C obtained using umbrella sampling with hard windows. Still the barrier is only around 2 $k_B T$ high, nevertheless we continue by investigating the transition mechanism.
To assess whether the size of the largest cluster N_c is a suitable reaction coordinate committor calculations have been performed. The results are shown in figure 5.11a as a function of the number of spins in the largest cluster of the system. As one can see the model function

$$P_{\mathcal{B}}(N_c) = \frac{1}{2}\left(1 + \tanh(\alpha_1 N_c + \alpha_0)\right), \tag{5.17}$$

where α_1 and α_0 have been determined using the likelihood maximization scheme de-

[6] Every cluster that is larger than this size is accounted for by a cluster that was identified to be the largest cluster in the system and there are no excess clusters.
[7] For example fitting the values from 70 to 118 yields a value of 0.8 and naturally reproduces the curve better for larger clusters

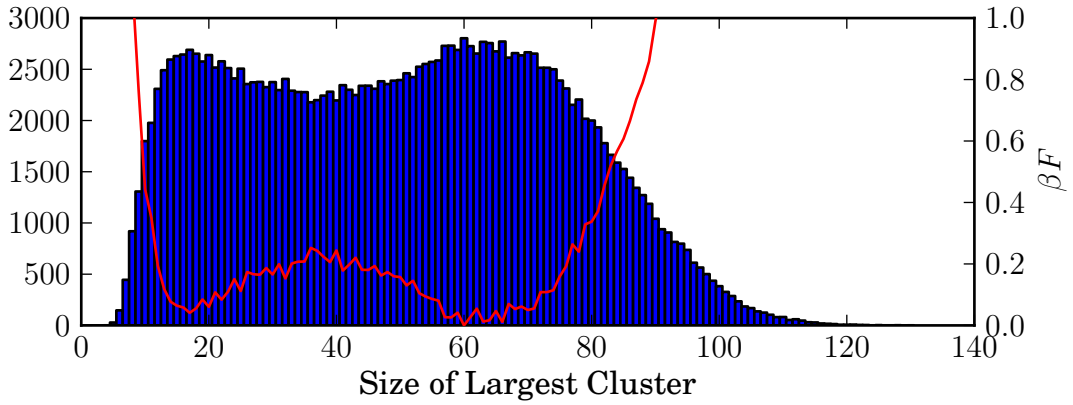

Figure 5.8.: Histogram of sizes of the largest cluster for a 100×100 spin square lattice Ising system at a constant magnetization of 0.961 and temperature 0.7 T_C. The red line shows the corresponding Landau free energy which has been shifted such that the minimum is 0.

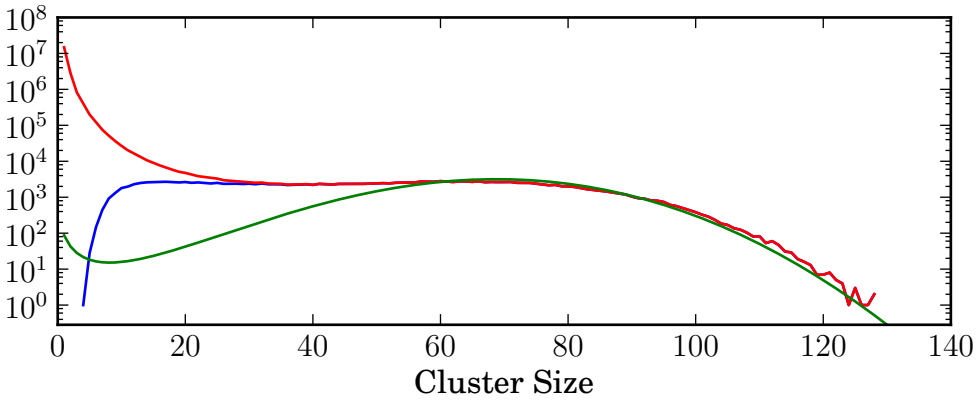

Figure 5.9.: Results obtained from a simulation at constant magnetization of 0.961 at temperature 0.7 T_C for 100×100 system. Shown are a histogram of cluster sizes found considering every cluster found in the simulation (red), a Histogram of cluster sizes considering only the largest cluster found within a given configuration (blue) and a fit of the model (5.13) using γ and an arbitrary shift as parameters (green). The other parameters necessary have been fixed using the equilibrium values calculated before (see figure 5.6) and the fit is carried over cluster sizes ranging from 50 spins to 118 spins. The fit shown yields a value of 0.89 kT per length for the surface tension γ.

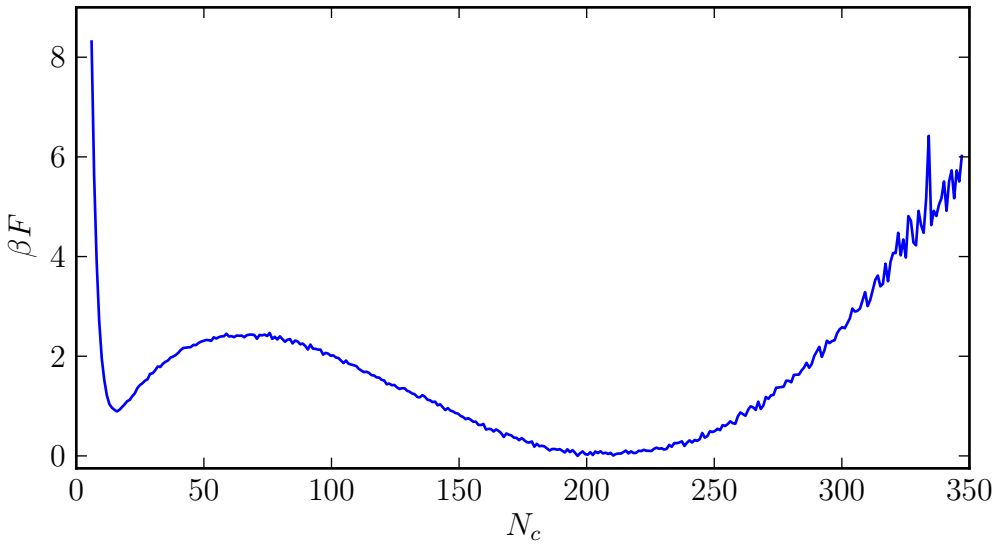

Figure 5.10.: Dimensionless free energy as a function of the size of the largest cluster in a 256×256 Ising system at temperature 0.7 T_C at magnetization 0.972. The data has been obtained in an umbrella sampling run with hard windows and 10^7 passes each. Exchanges of neighboring windows have been attempted every 10^3 passes.

scribed earlier, already describes the commitor fairly well. The critical cluster size is

$$N_c^* = 100. \tag{5.18}$$

A histogram test (figure 5.11b) performed with 1000 initial configurations taken from an umbrella sampling run using non-neighbor dynamics confirms this intuition yielding an intrinsic root mean square difference of the commitor surface of

$$\sigma_N = 0.066 \pm 0.003$$

with a mean probability of

$$\mu_N = 0.496 \pm 0.001.$$

To elucidate whether other order parameters can be used to improve the reaction coordinate figure 5.12 shows a collection of coordinates as a function of the largest cluster of the system as well as the corresponding commitor. From these plots alone none of the chosen coordinates seems to have a significant impact on the commitor. However a likelihood maximization again using a tanh model function suggests that combining the size of the largest cluster with its surface yields an improved reaction coordinate.
A visual inspection of the commitor as function of the combined coordinate, shown in figure 5.13a, however shows no significant improvement. The linear combination of the two variables obtained from likelihood maximization is given by

$$c = 0.0161V + 0.0198S - 2.39876 \tag{5.19}$$

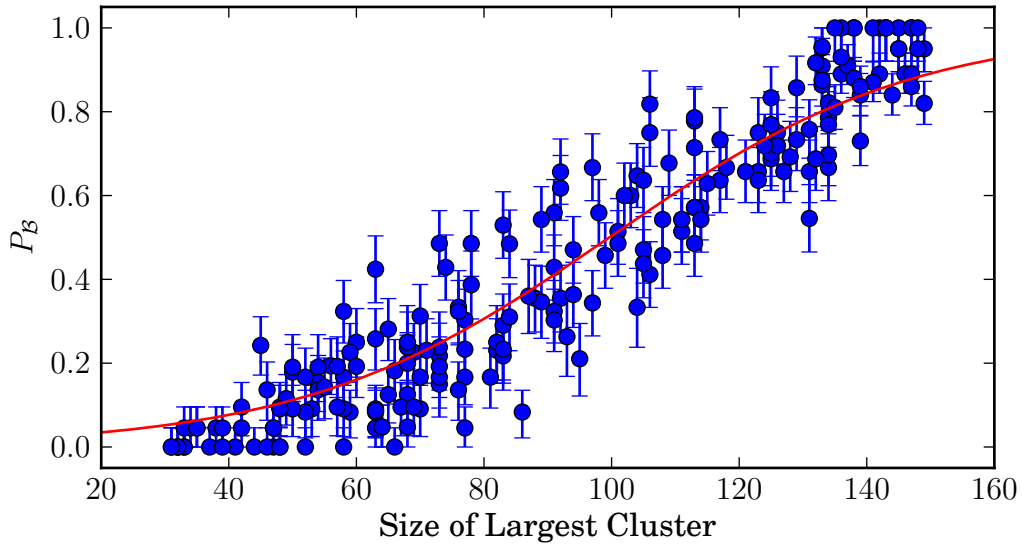

(a) Commitor probabilities as a function of the size of the largest cluster in the system. The red line is a solution to the maximum likelihood problem using the model (5.17) with a log-likelihood of −3046.3.

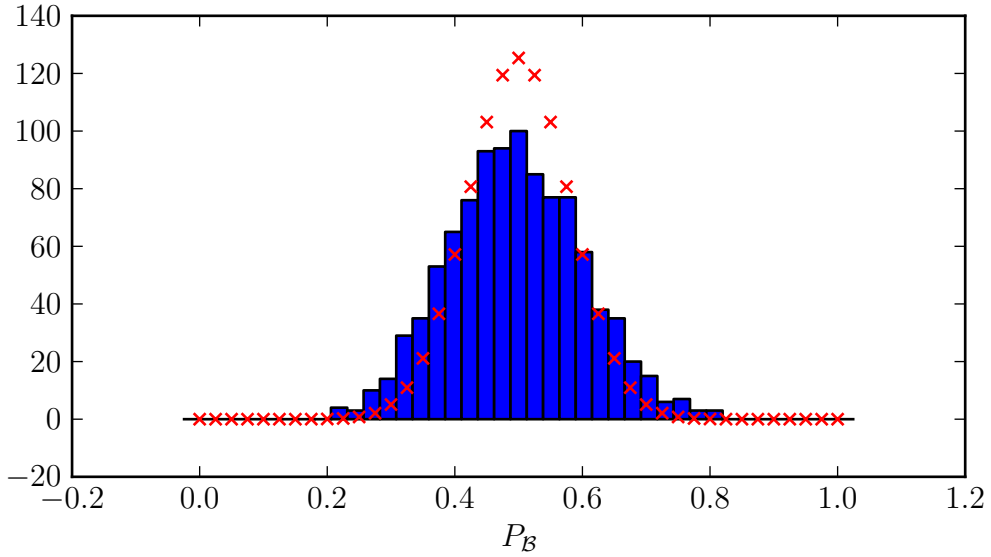

(b) Histogram test with configurations which contain a critical largest cluster with 100 spins. The red crosses indicate the expected counts if the probabilities were binomially distributed with a probability of 1/2.

Figure 5.11.: Commitor calculations and histogram test calculated in a 256×256 Ising system at temperature 0.7 T_C and magnetization 0.972. Configurations with a cluster that contains more than 150 spins are assumed to be in the droplet region, configurations where the largest cluster contains less than 20 spins are assumed to be in the homogeneous phase. The initial configurations have been obtained using umbrella sampling with hard windows using non-neighbor dynamics. In the commitor calculations neighbor dynamics have been used.

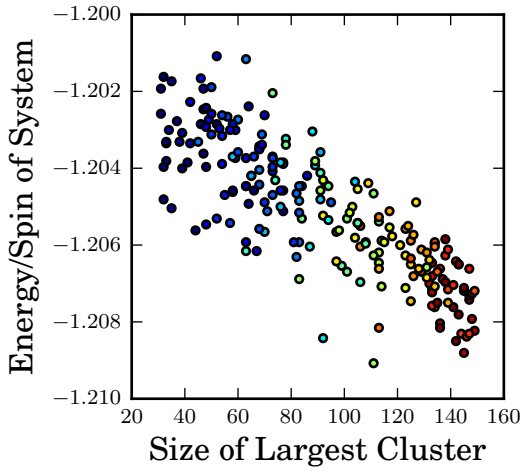

(a) Dimensionless Energy per spin as a function of cluster size.

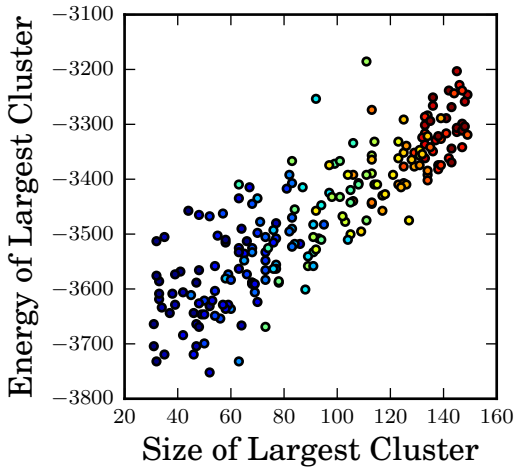

(b) Sum of energy contributed to the total energy by the spins that belong to the largest cluster of the system as a function of the size of largest cluster. This quantity is linearly dependant on the surface of the cluster.

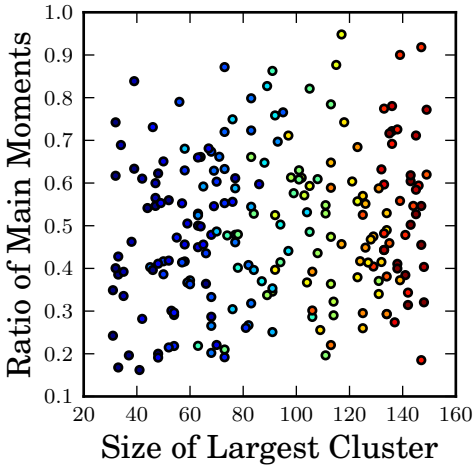

(c) Ratio of principal moments of inertia of the largest cluster of the surface as function of the size of the largest cluster. The principal moments of inertia are calculated as described in section 5.3.5.

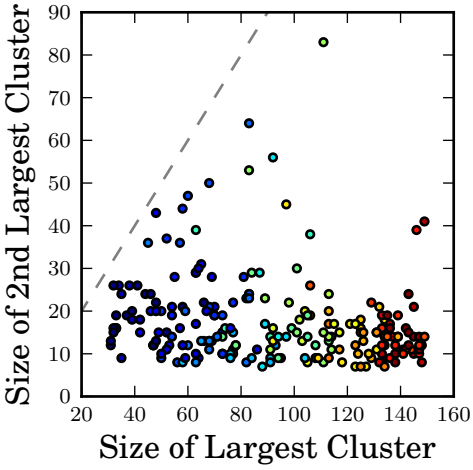

(d) Number of spins in the second largest cluster of the system as a function of the size of the largest cluster in the system. The line of equal size is shown in grey.

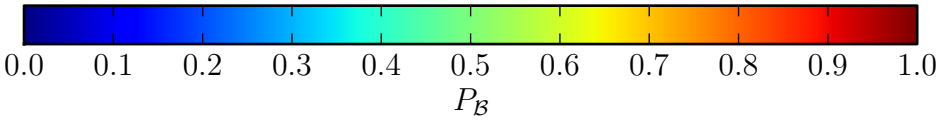

Figure 5.12.: Various order parameters as function of the size of the largest cluster in the 256×256 system for the set of configurations used in the initial calculation of commitor probabilities shown in figure 5.11a. Colors indicate the commitor probability $P_{\mathcal{B}}$.

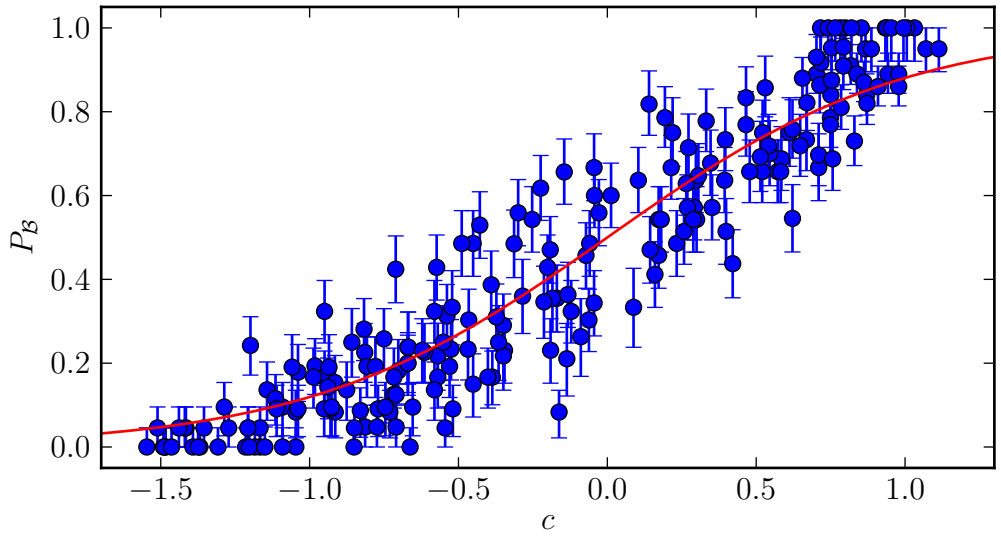

(a) Commitor probabilities as a function of the combined reaction coordinate c (5.19) in a given configuration calculated in a 256×256 Ising system at temperature 0.7 T_C. The red line shows the model probability $0.5*(1+\tanh(c))$ which gives a log-likelihood of the model of −3033.1.

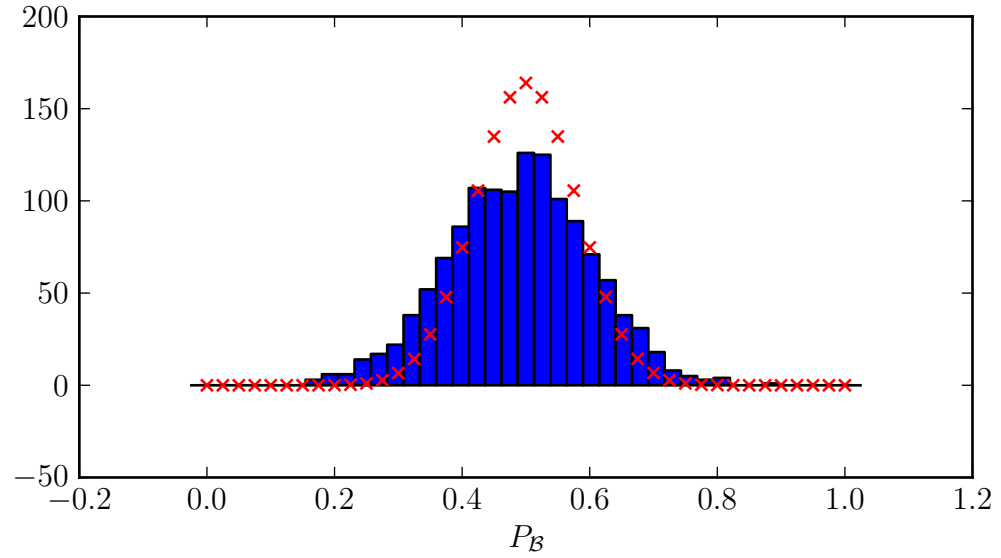

(b) Histogram test with configurations that exhibit a coordinate c in the interval $(-0.05, 0.05)$ for a 256×256 system at temperature 0.7 T_C and magnetization 0.972. For each probability 40 trajectories have been calculated. The red crosses indicate the expected counts if the probabilities were binomially distributed with a probability of $1/2$.

Figure 5.13.: Commitor calculations and histogram test for the combined coordinate c (5.19) calculated in 256×256 Ising system at temperature 0.7 T_C and magnetization 0.972. Configurations with a cluster that contains more than 150 spins are assumed to be in the droplet region, configurations where the largest cluster contains less than 20 spins are assumed to be in the homogeneous phase. The initial configurations have been obtained using umbrella sampling with hard windows using non-neighbor dynamics. In the commitor calculations neighbor dynamics have been used.

where the size of the cluster is denoted by V and the surface by S. A second histogram test is performed with 1308 different configurations and the results are shown in figure 5.13b. It yields an intrinsic mean square deviation of

$$\sigma_c = 0.075 \pm 0.003 \tag{5.20}$$

with a mean probability of

$$\mu_c = 0.489 \pm 0.001. \tag{5.21}$$

5.2.5. Discussion

The evaporation condensation transition in the 2D Ising model is theoretically rather well understood. In an attempt to reproduce the free energy observed we have used a CNT inspired model which we fitted towards the free energy obtained in simulation to obtain estimes for the surface tension. This estimate, although somewhat dependant on the exact procedure chosen, yields a slightly higher surface tension than the planar surface tension observed in simulation and obtained from analytic considerations casting doubt on the use of the planar interface tension for clusters of this small size.
Looking at possible reaction coordinates we have established that the size of the largest cluster describes the transition very well and, in contrast to cluster nucleation through the whole system, that the surface and the shape of the cluster seemingly can not be used to improve the reaction coordinate at least at this system size.
The likelihood maximization scheme used however suggested that such an improvement was possible. One can assume that this has to do with the inflexibility of the chosen model function which does not allow us to replicate the commitor distribution well enough. This brings out an important caveat in the maximum likelihood scheme used; the model function chosen has significant influence on the outcome of the optimization which makes the use of the Bayesian significance criterion introduced in section 4.3 more complicated. One may have to use a model with more degrees of freedom such as the string method proposed by Lechner et al. [39] accepting the computational difficulties associated. This result also underscores the importance of the histogram test in judging the quality of a given reaction coordinate.

5.3. Sphere to Slab Transition

5.3.1. Previous Results

The droplet strip phase transition has previously been studied in the context of surface tension calculations where the interfaces of the slab face have been used to calculate planar interface tensions [40, 41], as well as in connection with the exponential slowing down of multicanonical simulations [3]. Leung and Zia [11] calculated the minimum energy configuration for a droplet with fixed width L in the infinite volume limit to be a lens shape as shown in figure 5.14. We shall develop a similar model using an elliptical shape in section 5.3.2. Neuhaus and Hager [3] compared this prediction to simulation by doing a

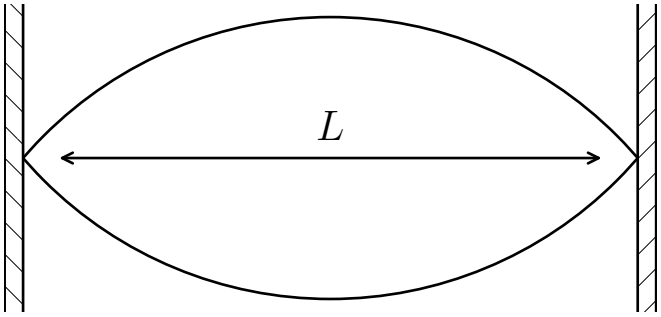

Figure 5.14.: Minimum surface configuration of a cluster with given extent L in one direction for a fixed volume as given by Leung and Zia [11]. The two surfaces are arcs of a circle. At slab-droplet coexistence the excess surface of a droplet with L equal to the width of the simulation box is calculated to be 13.46%.

finite size extrapolation of the barrier height between the two states. They find an excess free energy of (13.3 ± 0.6) % in good agreement with the theoretical prediction of Zia and Leung. To do so they introduced an order parameter by measuring the extent of a given cluster parallel to the x- and y-direction of the box. If theses lengths are L_1 and L_2 the order parameter is then given by

$$O = \frac{\max(L_1, L_2)}{L}, \tag{5.22}$$

where L is the length of the box wall.
This order parameter has the disadvantage that all configurations that contain a cluster that spans the simulation box are lumped together into a single bin of a histogram as a function of the order parameter. In the following sections we will develop order parameters that also distinguish between different spanning cluster configurations and hence allow us to sample both regimes of the transition.

5.3.2. Analytical estimate of energy barrier

We will first consider a model for the slab to sphere phase transition in which the cluster is deformed via a succession of ellipses that are cut off at the box border (see figure 5.15). During the transformation the area of the ellipse is kept constant, which corresponds to constant size of the cluster. At fixed area A and box size l the transition will be parametrized using the ratio q of semi-minor axis b to the semi-major axis a. Our artificial cluster transforms from a rectangle to a sphere if we vary q from 0 to 1.
We want to estimate the excess in surface the cluster experiences while changing its shape from the perfect sphere to the perfect rectangle. To do so we express the surface (i.e. the circumference) of our cluster in terms of A,l and q.

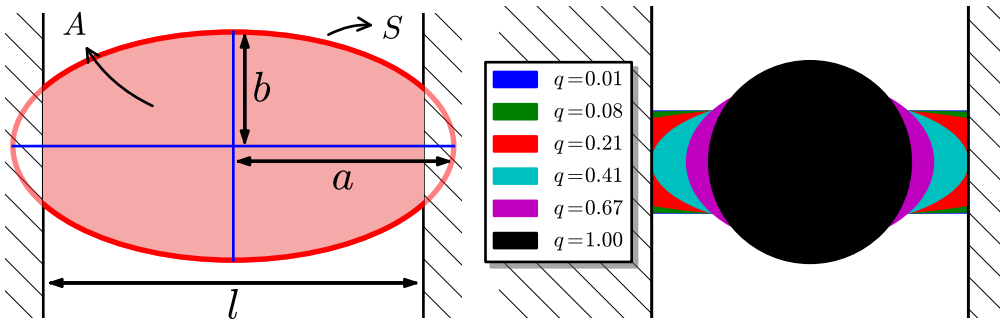

Figure 5.15.: Ellipses with different values $q = b/a$ as a model for the slab-spherical phase transition.

The circumference of this object is given by

$$S = 4a \int_0^{\varphi} \sqrt{1 - (1 - q^2) \sin^2 \varphi'} \, \mathrm{d}\varphi', \tag{5.23}$$

where a is the, as of yet unknown, semi-major axis and

$$\varphi = \begin{cases} \arcsin(l/2a) & \text{for } a > l/2 \\ \pi/2 & \text{for } a \leq l/2 \end{cases}. \tag{5.24}$$

The two domains $a > l/2$ and $a \leq l/2$ correspond to the cases where the cluster touches its counterpart in the neighboring box and where it does not. The limiting case is given by the ellipse with $a = l/2$ which is also the point of maximum surface. We can express this criterion in terms of A,l and q by using the area of this ellipse:

$$A = \pi ab = \pi q a^2 \text{ for } a \leq \frac{l}{2} \tag{5.25}$$

$$\frac{l}{2} = a = \sqrt{\frac{A}{\pi q}} \Leftrightarrow q_{\max} = \frac{4A}{l^2 \pi}. \tag{5.26}$$

By recognizing that for values $q \leq q_{\max}$ the ellipse touches its counterpart in the neighboring box, we can express the area A for all values of q:

$$A(a, q) = \begin{cases} \pi q a^2 & \text{for } q \geq 4A/(l^2\pi) \\ 4qa \int_0^{l/2} \sqrt{1 - \frac{x^2}{a^2}} \, \mathrm{d}x & \text{for } q < 4A/(l^2\pi) \end{cases}. \tag{5.27}$$

So for $q \geq 4A/(l^2\pi)$ a is simply given by $\sqrt{A/(\pi q)}$; for $q < 4A/(l^2\pi)$ however we have to solve the equation

$$\frac{A}{4q} = a \int_0^{l/2} \sqrt{1 - \frac{x^2}{a^2}} \, \mathrm{d}x \tag{5.28}$$

which involves an elliptic integral. By numerically solving (5.28) we obtain the function $a(q)$ which together with (5.23) and (5.24) gives the circumference S as a function of q.
Neglecting entropic effects for the time, we expect the surface of the perfect slab and the perfect circle to be equal at coexistence, which allows us to calculate the magnetization at coexistence m_{coex} (N being the total number of spins in the system):

$$2l = 2r\pi \Leftrightarrow r = \frac{l}{\pi} \tag{5.29}$$

$$A_{\text{coex}} = r^2\pi = \frac{l^2}{\pi} \tag{5.30}$$

$$m_{\text{coex}} = 1 - 2\frac{A_{\text{coex}}}{N} = 1 - \frac{2l^2}{\pi N}^{8} \tag{5.31}$$

For a rectangular grid l^2 is equal to N and therefore $m_{\text{coex}} = 1 - 2/\pi \approx 0.36$[9].
Figures 5.16a and 5.16b show the surface as a function of the magnetization and q or the Minimum Distance/Width D (see section 5.3.4 for a detailed definition) respectively as well as the surface as a function of q or D at fixed m_{coex}.
Furthermore we can estimate the height of the energy barrier by inserting the conditions for the cluster touching the box $a = l/2$ and $\varphi = \pi/2$ into equation (5.23) and calculating the ratio to the minimum surface $2l$ which yieelds the excess surface ratio

$$Q_{\text{exc}} = \int_0^{\pi/2} \sqrt{1 - (1 - \bar{q}_{\text{max}}^2)\sin^2\varphi'}\, \mathrm{d}\varphi' \approx 114\%, \tag{5.32}$$

where $\bar{q}_{\text{max}}$ is the value of q_{max} at coexistence which is calculated by inserting (5.30) into (5.26), yielding

$$\bar{q}_{\text{max}} = \frac{4}{\pi^2}. \tag{5.33}$$

Hence in this model the height of the energy barrier at coexistence is given as 14% of the surface of the perfect spherical or slab cluster and therefore scales linearly with the length of the box walls. This estimate is about 0.5% higher than the one given by Leung and Zia [11].

5.3.3. Simulation parameters

For the transition from spherical to slab configurations simulations at temperature 0.9 T_{C} and constant magnetization of 0.28 have been performed.
Free energy calculations were carried out using non-neighbor dynamics to take advantage of the higher transition rates ($\approx 5-10$ times higher) which improve sampling considerably.

[8] Note that we assumed to have a cluster with orientation -1. For the opposite orientation this expression is multiplied by -1.

[9] This calculation of m_{coex} is actually independant of any assumptions we made with regard to the transition mechanism.

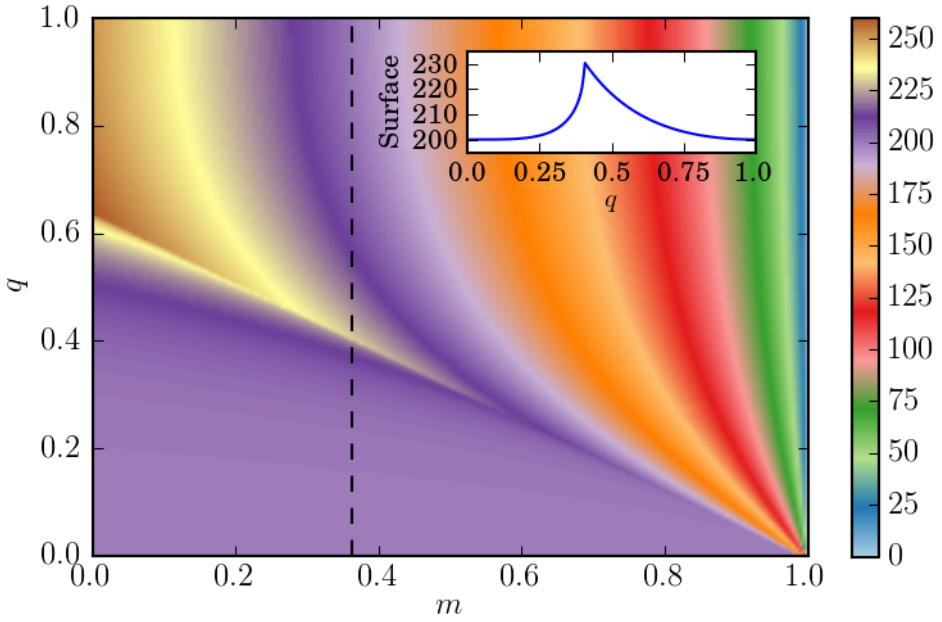

(a)

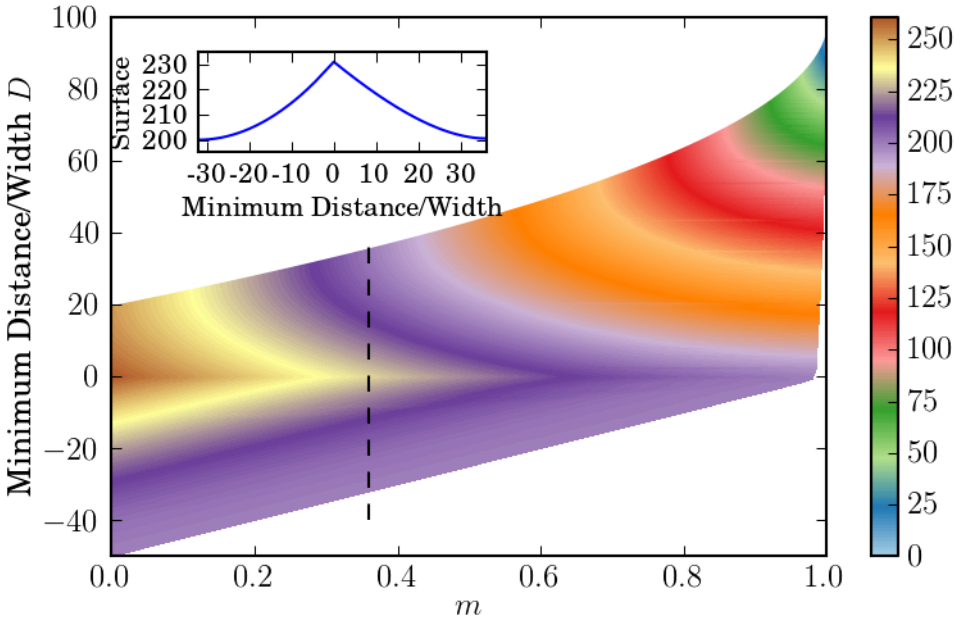

(b)

Figure 5.16.: Surface of elliptic cluster (a) as a function of $q = b/a$ where a,b are the semi-major and semi-minor axis respectively; (b) as a function of the Minimum Distance/Width D as described in section 5.3.4. The insets show the Surface as a function of either q or D at magnetization $m_{\text{coex}} = 1 - 2/\pi$ which is indicated by the dashed line.

Commitor calculations however have been performed using nearest neighbor moves since they, due to their local nature, resemble the processes in realistic models more closely. This should aid in transferring the results to other systems. The regions $\mathcal{A}$ and $\mathcal{B}$ are determined by defining value ranges for the order parameter D described in the next chapter. These have to be chosen for each temperature and magnetization seperately (see table 5.1) in order to avoid recrossings and at the same time limit the computational effort needed to calculate the probabilities. For the purpose of plotting the commitor distribution as a

T/m	0.9 T_C / 0.280
Region $\mathcal{A}$	$D < -15$
Region $\mathcal{B}$	$D > 15$

Table 5.1.: Definition of regions $\mathcal{A}$ and $\mathcal{B}$ in terms of order parameter D used in commitor calculations. $\mathcal{A}$ contains the slab and $\mathcal{B}$ the spherical configurations.

function of some proposed reaction coordinate, the number of trajectories generated was chosen such that the uncertainty of the probability, which is estimated using

$$\Delta p = \sqrt{\frac{p(1-p)}{N}} \tag{5.34}$$

where N is the number of trajectories, is below a given threshold. To ensure sufficient statistics a minimum of 10 simulations is performed for each initial configuration [16, 20]. For histogram tests this number is fixed. The commitor distributions shown during the initial assessment of proposed reaction coordinates were generated from a single set of simulations.

5.3.4. Minimum Distance - Minimum Width

As a possible reaction coordinate and to distinguish spherical configurations from Slab configurations we consider the following quantity D:

- Looking at the periodic copies of the largest cluster in the system, we construct the shortest distance from the original cluster to each of them and subsequently choose the smallest connection.[10]
- If this connection is bigger than 1, the cluster does not span the simulation box and we can directly use this distance as a measure for how "spherical" a cluster is. In this case
  $$D = \text{Length of shortest connection to periodic images.}$$
- If the shortest connection has length one, the cluster is connected to its periodic images and is therefore considered a spanning cluster. Furthermore we know to

[10] Some of the periodic images will yield the same distance and therefore need not be calculated. In 2 dimensions this reduces the number of distinct distances to 4.

which of its images the cluster is connected which defines a direction d. We now look at the largest cluster of opposite spin orientaion C_1 and its image in the direction orthogonal to d C_2. We choose

$$D = - \text{ Length of the shortest connection between } C_1 \text{ and } C_2.$$

This procedure essentially yields the shortest connection between the two surfaces of the cluster[11].

Figure 5.17 shows two examples of this construction. Since the minimum distance that a non-spanning cluster can have to one of its copies is $\sqrt{2}$ and the minimum width of a spanning-cluster that will be calculated above is 2, values in the interval $-2 < D \leq 1$ will not arise. The details of calculating the minimum distance between two sets of spins can be found in Appendix A.

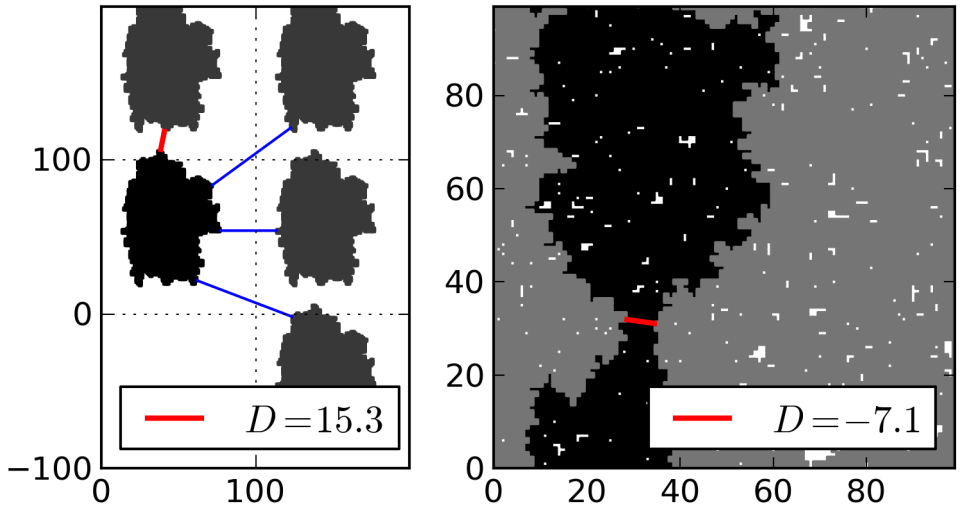

(a) (b)

Figure 5.17.: Examples of construction of the minimum distance/width coordinate D. (a) shows a non-spanning cluster and four of its periodic copies. The lines indicate a shortest connection to each one of them (which may not be unique) and the red line is the shortest one. The simulation box and its copies are indicated by dotted lines. (b) shows a spanning cluster (black) and its counterpart with opposite spin orientaion (gray). The red line indicates the shortest connection between the two adjacent clusters. The length of this connection is used to define D for spanning clusters.

In order to test whether the coordinate D distuingishes well between the slab and the spherical phase, simulations at constant magnetization at a temperature of 0.9 T_C and a magnetization of 0.28 have been performed (see Fig. 5.18). The histogram 5.18b shows that

[11] i.e. the minimum width of the cluster

D seperates two regions with the maximum free energy being located around 0. In figure 5.19 two sample configurations at equlibrium values of D are shown which demonstrate that D indeed serves as an order parameter for the slab-sphere transition.

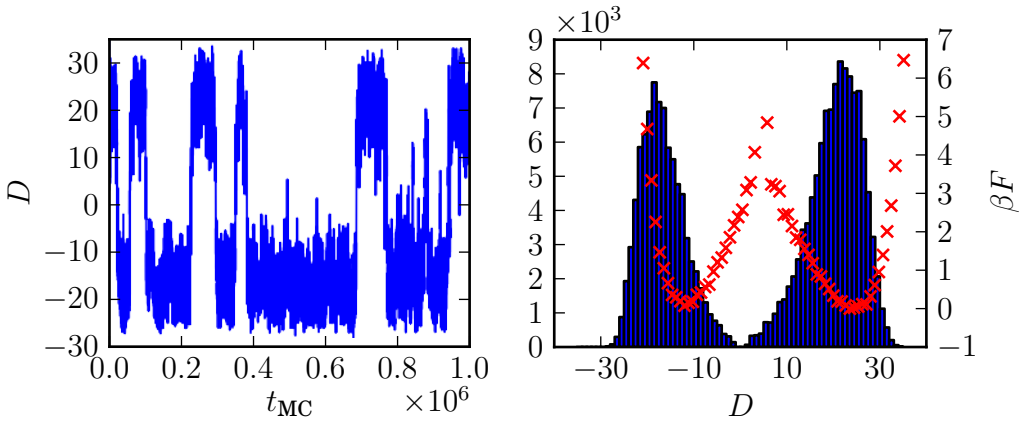

(a) (b)

Figure 5.18.: Data collected from a simulation of a 100×100 system with constant magnetization of 0.28 at a temperature of 0.9 T_{C} using non-neighbor dynamics. 10^7 passes have been performed of which only the first 10^6 are shown in (a) for clarity. At this temperature transitions between the slab- and the spherical-Phase are frequent enough such that no umbrella sampling is necessary. (a) shows the order parameter D as a function of the Monte-Carlo time and (b) a histogram of the values of the order parameter D encountered. The red crosses indicate the Landau Free energy in units of $k_{\mathrm{B}}T$ which has been shifted such that the minimum is 0.

Figure 5.20 shows the commitor probability as a function of D. Although we find some dependence, for configurations close to 0 probabilities from 0 to 1 are possible and hence some other factors must play a role in determining them. Hence D, which characterizes the local shape of the cluster, is not a good reaction coordinate on its own.
Taking a look at some of the configurations (figure 5.21) one may intuitively conclude that a key ingredient seems to be the global shape of the cluster, which is why in the following we explore some ways to characterize this aspect.

5.3.5. Moments of Inertia

A natural choice when trying to distinguish spherical from non-spherical clusters is to use some quantity formed by the principal moments of inertia of largest cluster of the system. In particular, we look at the ratio of the smaller principal moment of inertia of the cluster to the larger one. For spherical clusters we expect this ratio to be close to one, whereas for non-spherical clusters we expect it to be closer to 0.

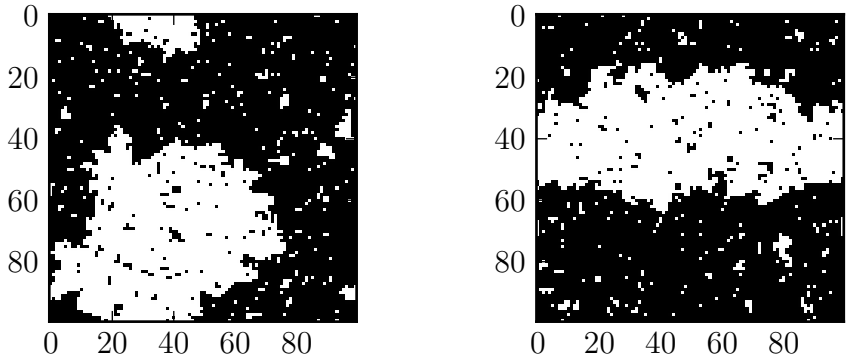

Figure 5.19.: Example spherical (left) and slab (right) configuration with D values of 22.8 and -20.9 respectively taken from simulations at temperature 0.9 T_C and constant magnetization of 0.28.

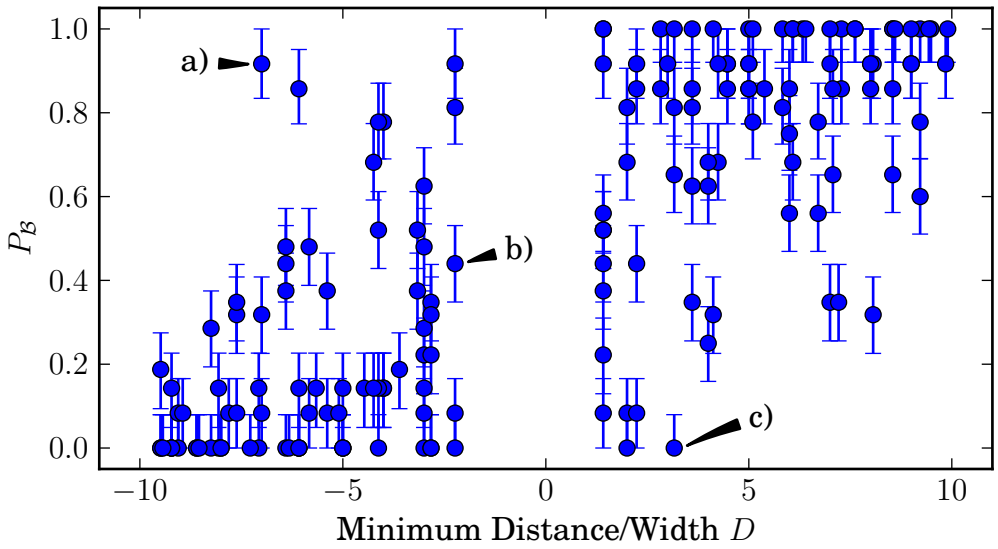

Figure 5.20.: Commitor probability $P_{\mathcal{B}}$ as a function of the parameter D. Simulations have been performed at constant magnetization of 0.28 in a Square Lattice Ising system with 100×100 spins at a temperature of 0.9 T_C. Region $\mathcal{B}$ contains the spherical configurations. The configurations marked with a,b and c are shown in figure 5.21. The gap in the D values observed is due to their construction that will not give values between -2 and $\sqrt{2}$.

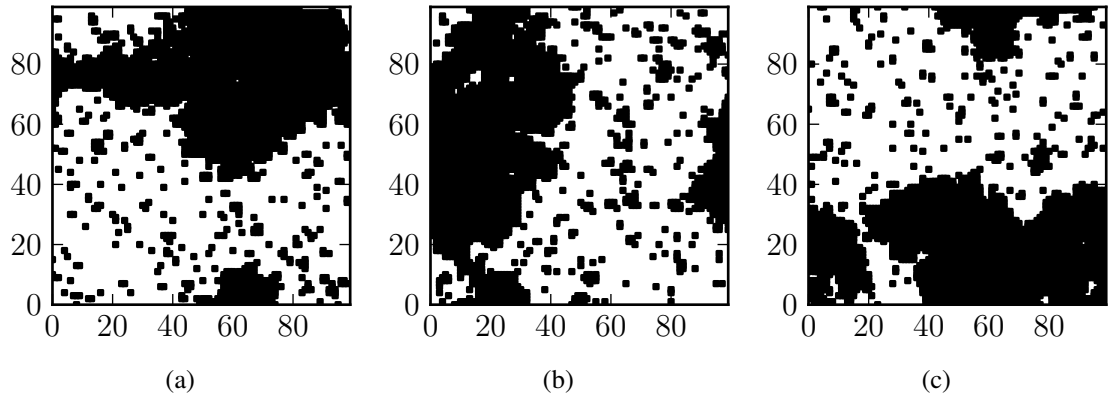

Figure 5.21.: Examples of configurations as marked in figure 5.20.

To make contact with our previous considerations we again look at perfectly elliptic clusters. The principal moments of inertia of an ellipse with a homogeneous mass distribution are given by

$$I = \frac{m}{5}\begin{pmatrix} b^2 & 0 \\ 0 & a^2 \end{pmatrix}, \tag{5.35}$$

and hence if we assume $b < a$ the mentioned ratio is given by

$$\alpha^2 = \frac{b^2}{a^2}. \tag{5.36}$$

Notice here that this α coincides with the quantity q used in section 5.3.2 for non-spanning elliptic clusters.
If we are given a cluster, where the periodic boundary conditions have already been taken care of, calculating α is straightforward. First of all we calculate the Center of Mass (CoM) using

$$\boldsymbol{r}_{\mathrm{CoM}} = \frac{1}{N}\sum_{i=1}^{N} \boldsymbol{r}_i \tag{5.37}$$

where $\boldsymbol{r}_i$ are the positions of each spin in the lattice and we assume that each spin has the same weight. Now we can calculate the symmetric inertia tensor given by

$$I = \frac{1}{N}\sum_{i=1}^{N}\begin{pmatrix} y_i^2 & -x_i y_i \\ -x_i y_i & x_i^2 \end{pmatrix}. \tag{5.38}$$

where

$$\begin{pmatrix} x_i \\ y_i \end{pmatrix} = \boldsymbol{r}_i - \boldsymbol{r}_{\mathrm{CoM}}. \tag{5.39}$$

The eigenvalues of this tensor are the principal moments of inertia.
In the discussion of how to assign coordinates to the spins in our cluster (see 5.1) we have already seen that in the case of spanning clusters we will not get unique results. In fact, the

calculation of α is in general ill defined for spanning clusters, since any translation of the cluster in the direction it spans the simulation box will change α (figure 5.22). Still, since

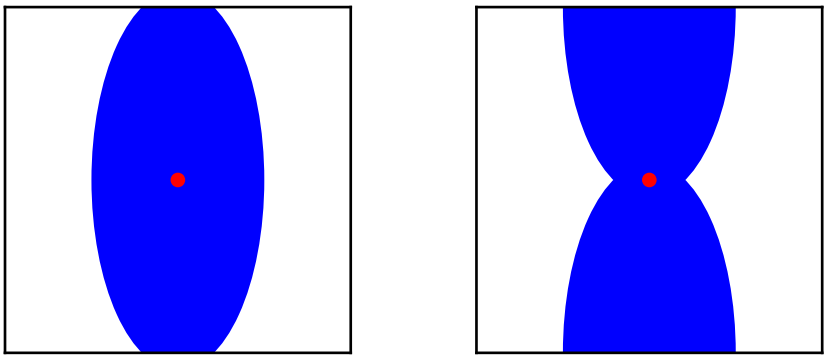

Figure 5.22.: Illustration of the problem of defining α such that its value is unique for a given spanning cluster. Shown are two elliptic clusters in a box with periodic boundary conditions. The cluster on the right has been shifted by half a box length into the y-direction and will lead to a different ratio of the main moments of inertia although from a physical point of view it represents the same cluster. The red dots indicate the calculated center of mass which serves as the reference point for the calculation of moments of inertia.

the procedure is well defined for spherical clusters, we can check whether this coordinate has any bearing on the commitor probability. To assess whether α serves as a good coordinate we first check whether we can distinguish spherical and slab configurations. To do so we look at a histogram of the values of α where we have used the previously defined quantity D to separate spanning from non-spanning clusters (figure 5.23). One can see that the quantity α distuingishes between two groups of configurations, however there is significant overlap of spanning and non-spanning clusters.

Furthermore we want to make sure, that α actually characterizes a different feature than D. To do so we plot the two parameters against each other for a set of configurations (figure 5.23a). We see that especially for spherical configurations for every value of D there is a wide range of α^2 values to be found and hence α^2 carries additional information.

In figure 5.24 we look at the commitor probabilities for spanning and non-spanning clusters seperately. Again we can immediately see, that α^2 has some bearing on whether a slab is formed or not, however for some values α^2 is not sufficient to determine the commitor of the configuration with any certainty. We conclude, that the global shape of the cluster, here characterized using α^2, is an independant feature which factors into the commitor probability. A good reaction coordinate will have to consider both the local and the global structure of the cluster.

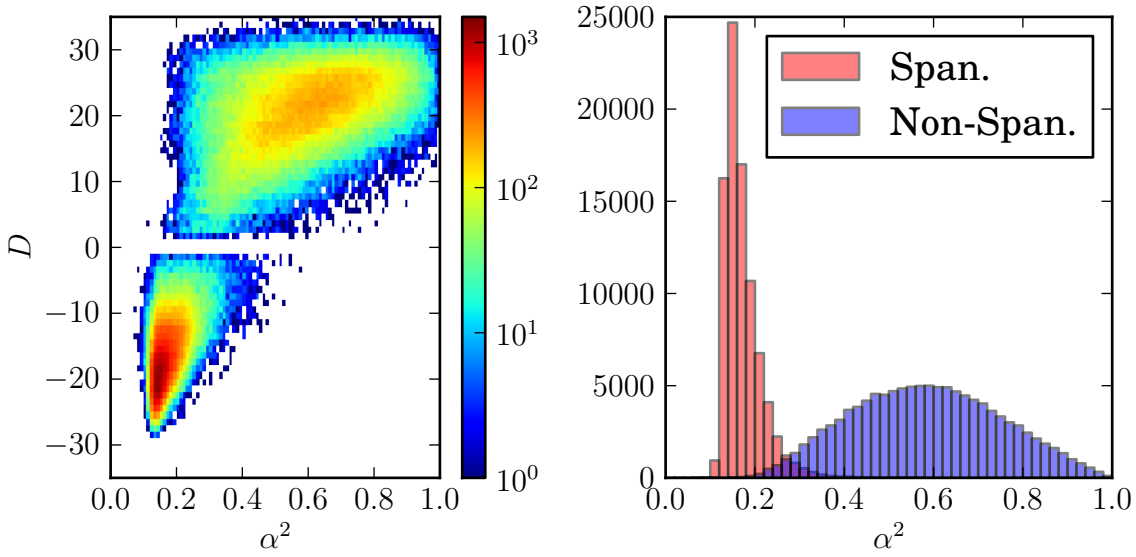

(a) (b)

Figure 5.23.: Histogram of values of α^2 collected from a simulation of a 100×100 Ising system at constant magnetization 0.280 and at a temperature of 0.9 T_C using non-neighbor dynamics. (a) shows a histogram of the values of D and α^2 encountered and (b) the projection onto the α^2 coordinate.

5.3.6. Using Fourier Transforms

We have previously seen that the global shape of the cluster, parametrized using the ratio of its principal moments of inertia α^2 influences the commitor of a given configuration, however it has proven to be difficult to consistently compute values of α for spanning clusters.

To address this issue we look at the Discrete Fourier Transform (DFT) of our configuration. Since it has periodic boundary conditions already built in, we might be able to find a coordinate that captures the global shape of the cluster and works for spanning as well as for non-spanning clusters.

To further motivate our choice of a possible reaction coordinate, we look at the 2D Fourier transform of a perfect slab and a perfectly spherical configuration. First we look at a slab of width Δx which we model by defining a density function

$$\rho_{\mathrm{sl}}(\boldsymbol{x}) = \theta\left(\frac{\Delta x}{2} - x\right) \tag{5.40}$$

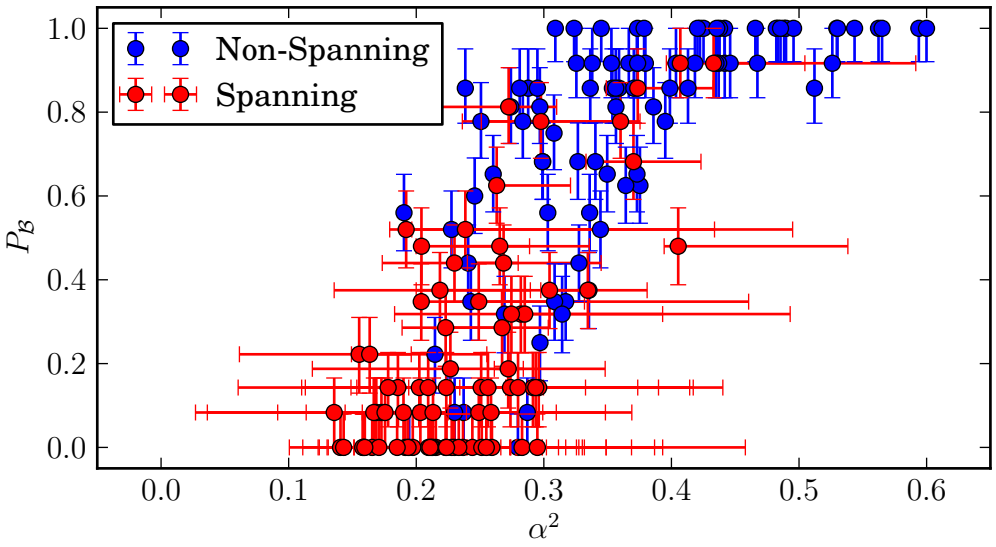

Figure 5.24.: Commitor probability $P_{\mathcal{B}}$ as a function of the parameter α^2. Simulations have been performed at constant magnetization of 0.280 in a Square Lattice Ising system with 100×100 spins at a temperature of 0.9 T_C using nearest neighbor dynamics. The definitions of $\mathcal{A}$ and $\mathcal{B}$ are shown in table 5.1 which result in region $\mathcal{B}$ containing the spherical configurations. The horizontal errorbars indicate the minimum and maximum value of α^2 that is found by translating the largest spanning cluster as shown in figure 5.22. The markers for non-spanning clusters are drawn at values that are calculated naively by choosing a random starting point for the reconstruction of the cluster.

where θ is the Heaviside distribution. The fourier transform is then calculated as follows:

$$\begin{aligned}\tilde{\rho}_{\mathrm{sl}}(\boldsymbol{k}) &= \int \mathrm{d}^2x\, \rho(\boldsymbol{x}) e^{-i\boldsymbol{k}\cdot\boldsymbol{r}} = \int_{-\infty}^{\infty} \mathrm{d}x \int_{-\infty}^{\infty} \mathrm{d}y\, \theta\left(\frac{\Delta x}{2} - x\right) e^{-i\boldsymbol{k}\cdot\boldsymbol{r}} \\ &= \int_{-\Delta x/2}^{\Delta x/2} \mathrm{d}x\, e^{-ik_x x} \int_{-\infty}^{\infty} \mathrm{d}y\, e^{-ik_y y} \\ &= \delta(k_y) \frac{2\sin(k_x \Delta x/2)}{k_x}\end{aligned} \tag{5.41}$$

A spherical configuration of radius R is given by

$$\rho_{\mathrm{sph}}(\boldsymbol{x}) = \theta(R - r) \tag{5.42}$$

and the corresponding fourier transform is given by

$$\tilde{\rho}_{\mathrm{sph}}(\boldsymbol{k}) = \int \mathrm{d}^2x\, \theta(R - r) e^{-i\boldsymbol{k}\cdot\boldsymbol{r}} = \frac{2\pi R}{k} J_1(kR) \tag{5.43}$$

where $k = |\boldsymbol{k}|$ and J_1 is the Bessel function of the first kind of order 1. As expected, the two Fourier Transforms are qualitatively different in that ρ_{sph} is spherically symmetric whereas ρ_{sl} is not. In the following we try to use this fact to construct a good reaction coordinate.
Since we are on a lattice in practice we of course have to use a discrete fourier transform which we define by setting

$$\tilde{\sigma}_{j,k} = \sum_{l=0}^{s_x-1} \sum_{m=0}^{s_y-1} \sigma_{l,m} \exp\left[-2\pi i \left(\frac{jl}{s_x} + \frac{km}{s_y}\right)\right], \tag{5.44}$$

where $\sigma_{l,m}$ is the value of the spin at position l, m in the lattice and s_x and s_y are the size of the lattice in the x and y direction respectively. The values of our spins are real (either $+1$ or -1) and therefore we know that

$$\tilde{\sigma}_{s_x-l,s_y-k} = \overline{\tilde{\sigma}_{l,k}}, \tag{5.45}$$

which allows us to only look at half the number of Fourier-Coefficients since the ones mirrored around the origin do not contain additional information.
We are mainly interested in the global shape of the cluster, so we look at the long wavelength k-vectors in the vicinity of the origin in k-space. In particular we look at the ratio

$$F = \frac{\max\left(\left|\tilde{\sigma}_{1,0}\right|, \left|\tilde{\sigma}_{0,1}\right|\right)}{\min\left(\left|\tilde{\sigma}_{1,0}\right|, \left|\tilde{\sigma}_{0,1}\right|\right)}, \tag{5.46}$$

which we expect to be close to 1 for spherical clusters and smaller than 1 for other shapes. In connection with the model chosen in section 5.3.2 figure 5.25 shows F for perfect ellipses that are cut off at the box walls as a function of $q = b/a$, the ratio of minor to major axis. The resulting function $F(q)$ is monotonic and as therefore a viable candidate as a reaction coordinate.
Since we only use the smallest k-vectors we expect influences of small fluctuations inside or around the cluster of interest to be suppressed and we therefore don't have to search for clusters. This fact together with the use of FFT make calculating F very efficient. The relationship between F and α^2 is established in figure 5.27 where we can see, that for spherical configurations the two parameters are correlated and therefore we may expect them to perform comparably as a reaction coordinate for non-spanning clusters and also it enables us to interpret F similar to α^2. The key advantage of F over α^2 is that it is also well defined for spanning clusters which allows for a better description of the cluster and will therefore hopefully aid us in constructing a reaction coordinate.
Again looking at a histogram of the values of F encountered during a simulation at temperatue 0.9 T_{C} (figure 5.26), we see that F for the most part seperates spanning from non-spanning clusters and that the free energy barrier is of the order of $2k_{\text{B}}T$. F seperates the slab configurations into more bins than the previously inspected α^2 which may aid in constructing a reaction coordinate from it.
The commitor distribution associated with F is shown in figure 5.28. As was previously the case with α^2, F is not able to predict the commitor probabibility for all values encountered.

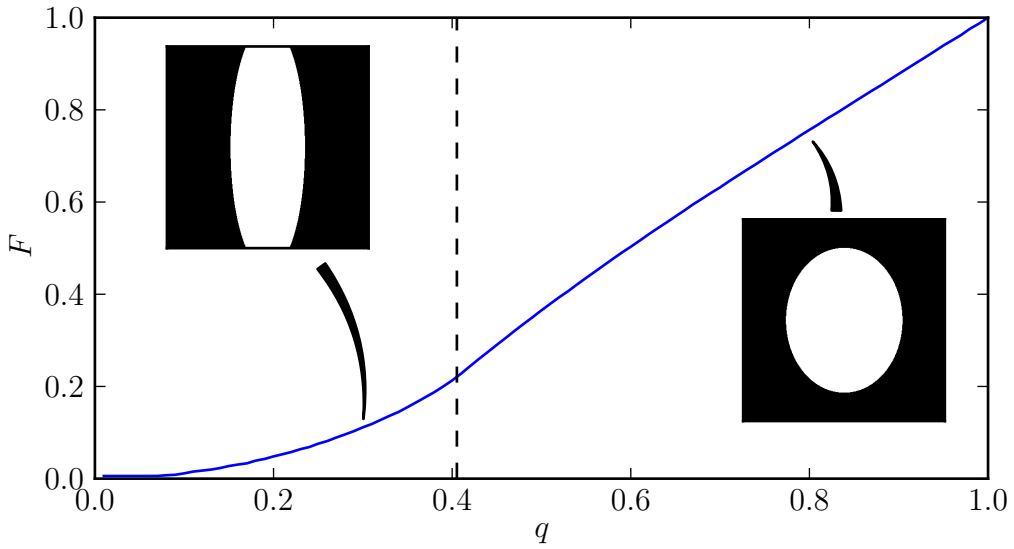

Figure 5.25.: Value of reaction coordinate F for perfectly elliptical clusters as a function of the ratio of minor to major axis q. For the calculation a quadratic box of length 400 has been used and the size of the cluster has been chosen to be consistent with a magnetization of 0.36. The dashed line indicates the q-value at which the cluster touches its counterpart in the next copy of the simulation box. The Fourier transform has been calculated using a fast fourier transform algorithm.

However the performance of the two parameters is comparable justifying the usage of F instead of α^2 in the following considerations.

5.3.7. Combining Minimum Distance/Width and Fourier Transforms

We have seen in sections 5.3.4 and 5.3.6 that D and F are partly capable of characterizing the transitions occuring between slab and spherical configurations. However both of them are not good reaction coordinates by themselves. Since they capture different aspects, a combination of these two coordinates is another obvious possibility.
Using the set of 135 commitor probabilities calculated at temperature 0.9 T_C previously shown, a likelihood maximization as shown in section 4.3 using the pairs of parameters D and F has been performed. The model function is given by

$$P_{\mathcal{B}}(r) = \frac{1}{2}(1 + \tanh(r)) \tag{5.47}$$

where r is a linear combination of the coordinates D and F:

$$r = \alpha_0 + \alpha_1 D + \alpha_2 F \tag{5.48}$$

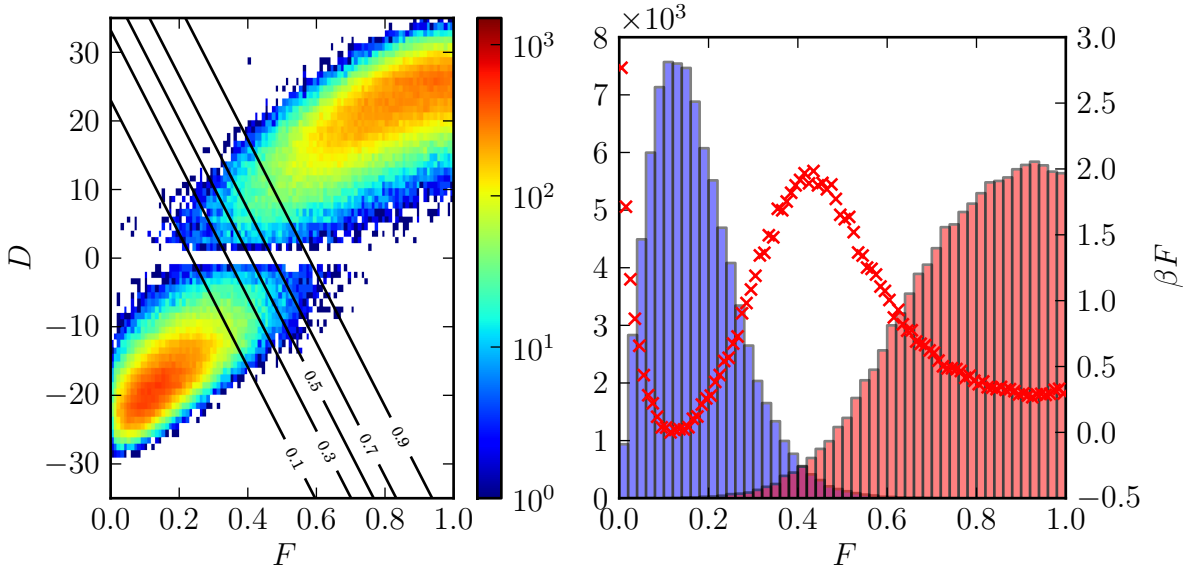

(a) (b)

Figure 5.26.: Data collected from a simulation of a 100×100 system with constant magnetization of 0.28 at a temperature of 0.9 T_C using non-neighbor Dynamics. 10^7 sweeps have been performed. At this temperature, transitions between the slab and the spherical phase are frequent enough such that no umbrella sampling is necessary. (a) shows a histogram of of the encountered value pairs of D and F. In black isocommitor lines for the reaction coordinate r (see section 5.3.7) are shown. (b) shows the projection on the order parameter F. Spanning clusters (blue) and non-spanning clusters (red) are shown separately. The red crosses indicate the Landau Free energy in units of $k_B T$ as a function of F which has been shifted such that the minimum is 0.

The optimization yields the result

$$r = -2.62 + 0.0662D + 6.44F \tag{5.49}$$

which leads to the commitor shown in figure 5.29. The corresponding isosurfaces have been drawn in figure 5.26a and the free energy as a function of r is shown in figure 5.30a. By construction, the critical value of r^* of r is 0. We can immediately see, that now the situation is much improved in the sense that for all values of r the range of probabilities encountered is limited.
To further assess the quality of r as a reaction coordinate, a histogram test with 922 configurations with values of r between -0.1 and 0.1, which translate to predicted commitor probabilities between 0.45 and 0.55, has been performed. The configurations have been gathered using a set of 4 simulations at constant magnetization using Nearest-Neighbor dynamics with 10^8 passes each. To allow for equilibration of the initially random configuration the first 2.5 10^6 passes have been discarded.

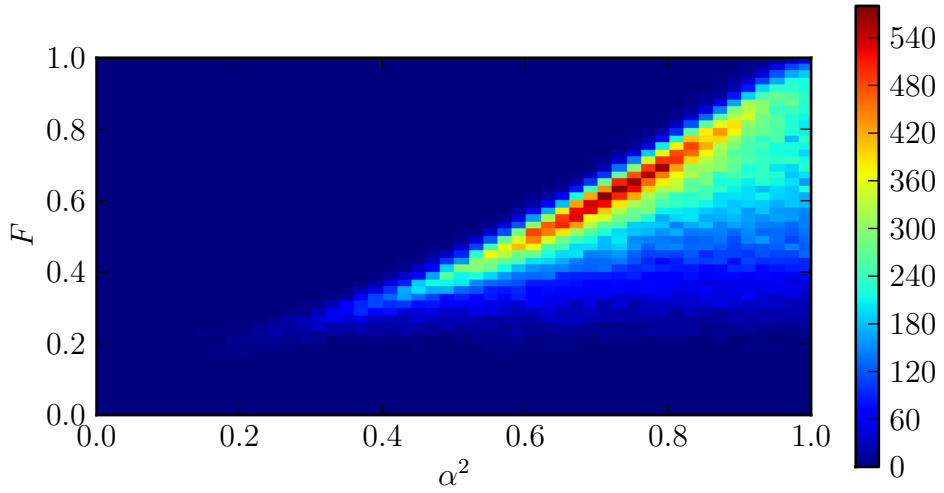

Figure 5.27.: Histogram of pairs of values α^2 and D encountered in a simulation at constant magnetization of 0.28 and a temperature of 0.9 T_C. The correlation of the two parameters allows us to interpret F as a measure for the "asphericity" of the largest cluster of the system.

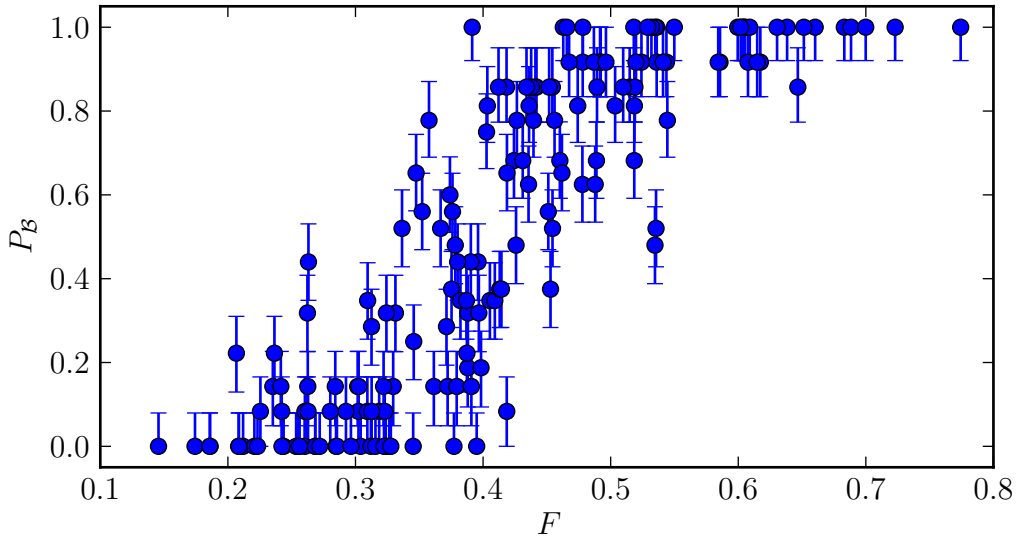

Figure 5.28.: Commitor $P_{\mathcal{B}}$ as a function of the parameter F. Simulations have been performed at constant magnetization of 0.280 in a Square Lattice Ising system with 100×100 spins at a temperature of 0.9 T_C using neighbor dynamics. The definitions of $\mathcal{A}$ and $\mathcal{B}$ are shown in table 5.1 which result in region $\mathcal{B}$ containing the spherical configurations.

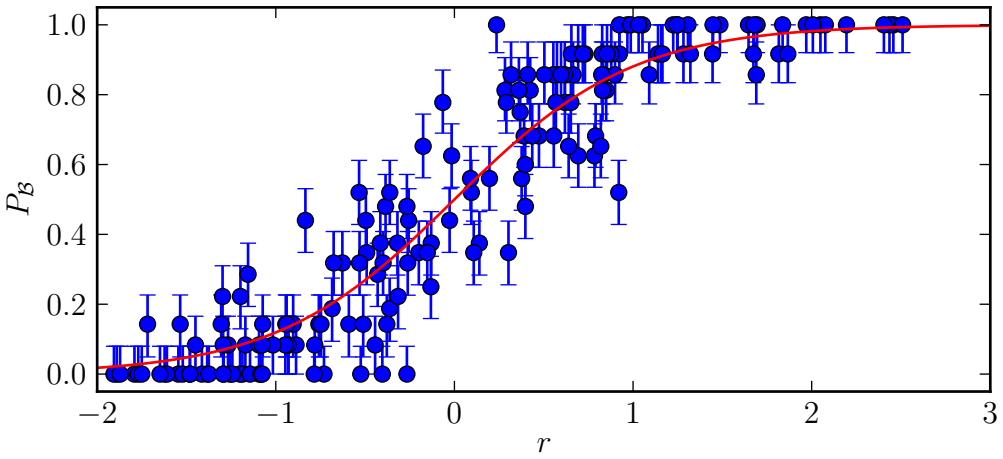

Figure 5.29.: Commitor obtained using the reaction coordinate r that contains contributions from coordinates D and F that have been combined using likelihood maximization. The commitor probabilities shown have been obtained at temperature 0.9 T_C and constant magnetization of 0.28. Nearest-Neighbor dynamics have been used. The data points shown are the ones used to determine the coefficients in equation (5.49). The red line represents the function $P_{\mathcal{B}}(r) = 0.5(1 + \tanh(r))$ used to define the likelihood.

The commitor probabilities of these configurations have been estimated using 30 trajectories each. Figure 5.30b shows the histogram of estimated probabilities. The intrinsic mean probability μ of the proposed isocommitor surface is estimated to be

$$\mu = 0.542 \pm 0.003,$$

and the intrinsic root mean square deviation σ equates to

$$\sigma = 0.107 \pm 0.005.$$

5.3.8. Discussion and open questions

We have developed order parameters for the 2D Ising model slab-sphere transition which are defined for both spanning and non-spanning clusters within a system which uses periodic boundary conditions. Furthermore we have found a suitable reaction coordinate by combining a coordinate defined as the minimum distance of a cluster to its periodic images or the minimum width of a slablike cluster with a coordinate that approximates the shape of the cluster based on a fourier transform of the configuration. The quality of the critical isocommitor surface calculated using the combined coordinate is significantly better than random given its lower intrinsic deviation from true isocommitor surface.
The fact that the Minimum Distance/Width coordinate on its own can not be used to accurately predict commitor probabilities but rather one has to use a shape parameter as well,

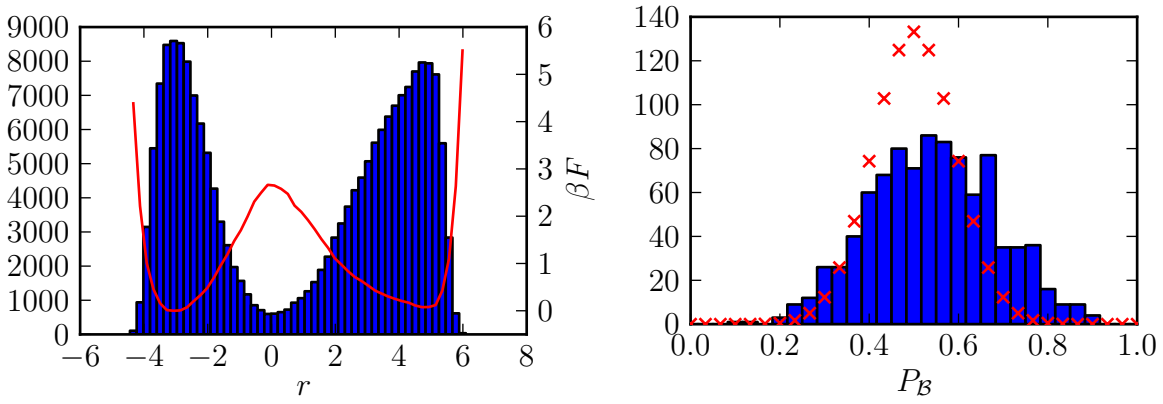

(a) (b)

Figure 5.30.: Assessment of possible reaction coordinate r using constant magnetization simulations at magnetization 0.28 and temperature 0.9 T_C. (a) shows a histogram of values of r encountered using Non-Neighbor dynamics and in red the corresponding dimensionless free energy, which has been shifted such that the minimum free energy is 0. (b) is a histogram of calculated commitor probabilities for initial configurations generated in simulations using Nearest-Neighbor dynamics. 922 configurations have been chosen such that the combined reaction coordinate r is within the interval $-0.1 \leq r \leq 0.1$. According to the model (5.47) we expect the commitor probabilities of these configurations to fall within the interval $0.45 \leq P_{\mathcal{B}} \leq 0.55$. The probabilities are estimated from 30 trajectories each generated using Nearest-Neighbor dynamics at a temperature of 0.9 T_C. Red crosses indicate the number of expected counts if the number of trajectories that commited to $\mathcal{B}$ was binomially distributed with probability $1/2$.

hints at the fact that at a rather high temperature of 0.9 T_C for a transition to occur the cluster not only has to build a connection to its periodic image but also the overall shape of the cluster has to be favorable. The temperature dependence of this relationship may be worth further study. In particular one may ask if at lower temperaturs the Fourier transform alone can be used as a reaction coordinate which would be favourable since its computation is very efficient.

For the minimum distance calculations an extension to three dimensions as well as to off-lattice system can be carried out easily. For the coordinates involving fourier transformations a generalization to 3 dimensions should be possible by defining suitable parameters for the sphere-cylinder and cylinder-slab transition. Transferring these methods to off-lattice systems likely requires some more work since one has to find a suitable replacement for the simple fourier transform of the configuration. Developing such a solution may allow efficient sampling of the geometric phase transitions in other systems.

6. Acknowledgements

Various software packages have been used throughout this work which shall be acknowledged in the following list.

- Qhull [42] has been used to calculate Delaunay Triangulations of point sets.
- FFTW [43] and FFTW++ (`fftwpp.sourceforge.net`) have been used for efficient calculation of fourier transforms
- Various convenience functions from the boost C++ Libraries (`www.boost.org`)
- NumPy and SciPy packages for calculations in Python (`www.numpy.org`)
- matplotlib (`matplotlib.org`) has been used for all the plots and diagrams in this work

A. Minimum Distance Calculations

The calculation of the minimum distance between two clusters of particles is a specialization of what is known as the problem of finding the bichromatic closest pair. It can be defined as follows:

> Given a set of n red and m green points in $\mathbb{E}^d$ find a red point r and a green point g such that the distance between r and g is minimum among all red-green pairs. [44]

In our specific problem the sets of red and green points become the two clusters. Furthermore we need the concept of a Euclidean minimum spanning tree:

> Given a set S of N points in Euclidean d-dimensional space $\mathbb{E}^d$, a *Euclidean minimum spanning tree* (EMST) is a spanning tree of S whose edges have a minimum total length among all spanning trees of S, where the length of an edge is the Euclidean distance between its vertices [44].

We can show by contradiction that the EMST of the union of red and green points must contain at least one shortest red-green pair.
Assume that we have an EMST $\mathcal{A}$ over the union of red and green points that does not contain a shortest red-green pair. Looking at one of the shortest red green pairs (r_s,g_s) that is connected by the edge $\mathcal{E}$, we can shorten the overall length of A by replacing one of the edges that connects either r_s or g_s to A with $\mathcal{E}$. Hence $\mathcal{A}$ can not be an EMST contradicting our previous assumption.
Calculating the *Minimum Spanning Tree* for a given graph is a well known problem in computer science, which has developed multiple solutions, one of them being *Prim's Algorithm*. To do so however we first have to calculate a graph for our clusters, that is a superset of the EMST. In the course of this work a Delaunay Triangulation has been used which generates a euclidean graph of the two clusters at hand that is known to be a superset of the EMST [45]. This graph is then either directly searched for the shortest connection, or, depending on the number of points involved, reduced to a minimum spanning tree which is then searched.
This procedure reduces the time complexity of the problem from the initial $\mathcal{O}(N^2)$ to $\mathcal{O}(N \log N)$. To further reduce the computational effort needed we can use the fact, that the two sets of points will never intersect with each other and we therefore only have to consider the elements of the cluster that are on its surface. A spin is considered to be on the surface of the cluster if one of its four nearest neighbors is not an element of the cluster.

List of Figures

Bibliography

1. Eckhardt, W. *et al.* 591 TFLOPS multi-trillion particles simulation on SuperMUC. *Supercomputing,* 1–12 (2013).
2. Frenkel, D. & Smit, B. *Understanding molecular simulation: from algorithms to applications* (Elsevier, Singapore, 2009).
3. Neuhaus, T. & Hager, J. S. Exponential Slowing Down in Simulations of First-Order Phase Transitions. *Journal of Statistical Physics* **113,** 47–83. doi:10.1023/A:1025718703965 (2003).
4. Ising, E. Beitrag zur Theorie des Ferromagnetismus. *Zeitschrift für Physik* **31,** 253–258 (1925).
5. Peierls, R. & Born, M. On Ising's model of ferromagnetism. *Mathematical Proceedings of the Cambridge Philosophical Society,* 477–481. doi:10.1017/S0305004100019174 (1936).
6. Kramers, H. A. & Wannier, G. H. Statistics of the Two-Dimensional Ferromagnet. Part I. *Phys. Rev.* **60,** 252–262. doi:10.1103/PhysRev.60.252 (1941).
7. Bragg, W. L. & Williams, E. J. The effect of thermal agitation on atomic arrangement in alloys. *Proceedings of the Royal Society of London. Series A* **145,** 699–730 (1934).
8. Onsager, L. Crystal statistics. I. A two-dimensional model with an order-disorder transition. *Physical Review* **737** (1944).
9. Yang, C. The Spontaneous Magnetization of a Two-Dimensional Ising Model. *Physical Review* **85,** 808–816. doi:10.1103/PhysRev.85.808 (1952).
10. Wulff, G. On the question of speed of growth and dissolution of crystal surfaces. *Zeitschrift für Kristallographie und Mineralogie* **34,** 449–530 (1901).
11. Leung, K & Zia, R. K. P. Geometrically induced transitions between equilibrium crystal shapes. *Journal of Physics A: Mathematical and General* **23,** 4593–4602. doi:10.1088/0305-4470/23/20/021 (1990).
12. Metropolis, N. *et al.* Equation of State Calculations by Fast Computing Machines. *The Journal of Chemical Physics* **21,** 1087. doi:10.1063/1.1699114 (1953).
13. Kawasaki, K. Diffusion Constants near the Critical Point for Time-Dependent Ising Models. I. *Physical Review* **145,** 224–230. doi:10.1103/PhysRev.145.224 (1966).
14. Ferrenberg, A. & Swendsen, R. Optimized Monte Carlo data analysis. *Physical review letters* **63,** 1195–1198 (1989).

15. Peters, B. & Trout, B. L. Obtaining reaction coordinates by likelihood maximization. *The Journal of chemical physics* **125,** 054108. doi:10.1063/1.2234477 (2006).

16. Bolhuis, P. G. *et al.* Transition path sampling: throwing ropes over rough mountain passes, in the dark. *Annual review of physical chemistry* **53,** 291–318. doi:10.1146/annurev.physchem.53.082301.113146 (2002).

17. Tuckerman, M. E. *Statistical Mechanics: Theory and Molecular Simulation* (Oxford University Press, New York, 2010).

18. Ma, A. & Dinner, A. R. Automatic method for identifying reaction coordinates in complex systems. *The journal of physical chemistry. B* **109,** 6769–79. doi:10.1021/jp045546c (2005).

19. Peters, B. Using the histogram test to quantify reaction coordinate error. *The Journal of chemical physics* **125,** 241101. doi:10.1063/1.2409924 (2006).

20. Grünwald, M. & Dellago, C. Transition state analysis of solid-solid transformations in nanocrystals. *The Journal of chemical physics* **131,** 164116. doi:10.1063/1.3253700 (2009).

21. Pan, A. C. & Chandler, D. Dynamics of Nucleation in the Ising Model. *The Journal of Physical Chemistry B* **108,** 19681–19686. doi:10.1021/jp0471249 (2004).

22. Peters, B. *et al.* Extensions to the likelihood maximization approach for finding reaction coordinates. *The Journal of chemical physics* **127,** 034109. doi:10.1063/1.2748396 (2007).

23. Hoshen, J. & Kopelman, R. Percolation and cluster distribution. I. Cluster multiple labeling technique and critical concentration algorithm. *Physical Review B* **14,** 3438–3445. doi:10.1103/PhysRevB.14.3438 (1976).

24. Flanigan, M. & Tamayo, P. Parallel cluster labeling for large-scale Monte Carlo simulations. *Physica A: Statistical Mechanics and its Applications* **215,** 461–480. doi:10.1016/0378-4371(95)00019-4 (1995).

25. Tiggemann, D. *Numerical methods for the determination of the properties and critical behaviour of percolation and the Ising model* PhD thesis (Cologne, Germany, 2007).

26. Mayer, J. E. & Wood, W. W. Interfacial Tension Effects in Finite, Periodic, Two-Dimensional Systems. *The Journal of Chemical Physics* **42,** 4268. doi:10.1063/1.1695931 (1965).

27. Schrader, M. *et al.* Simulation of vapor-liquid coexistence in finite volumes: A method to compute the surface free energy of droplets. *Physical Review E* **79,** 061104. doi:10.1103/PhysRevE.79.061104 (2009).

28. Tröster, A. *et al.* Numerical approaches to determine the interface tension of curved interfaces from free energy calculations. en. *The Journal of chemical physics* **136,** 064709. doi:10.1063/1.3685221 (2012).

29. Tröster, A. & Binder, K. Positive Tolman Length in a Lattice Gas with Three-Body Interactions. *Physical Review Letters* **107,** 265701. doi:10.1103/PhysRevLett.107.265701 (2011).

30. Binder, K. & Kalos, M. H. ?Critical clusters? in a supersaturated vapor: Theory and Monte Carlo simulation. *Journal of Statistical Physics* **22,** 363–396. doi:10.1007/BF01014648 (1980).

31. Biskup, M. *et al.* On the formation/dissolution of equilibrium droplets. *Europhysics Letters (EPL)* **60,** 21–27. doi:10.1209/epl/i2002-00312-y (2002).

32. Biskup, M. *et al.* Critical region for droplet formation in the two-dimensional Ising model. *Communications in mathematical physics* **183,** 137–183 (2003).

33. Rottman, C. & Wortis, M. Exact equilibrium crystal shapes at nonzero temperature in two dimensions. *Physical Review B* **24,** 6274–6277 (1981).

34. Zia, R. & Avron, J. Total surface energy and equilibrium shapes: Exact results for the d=2 Ising crystal. *Physical Review B* **25,** 2042–2045. doi:10.1103/PhysRevB.25.2042 (1982).

35. Nuß baumer, A. *et al.* Monte Carlo study of the droplet formation-dissolution transition on different two-dimensional lattices. *Physical Review E* **77,** 041109. doi:10.1103/PhysRevE.77.041109 (2008).

36. Nuß baumer, A. *et al.* Free-Energy Barrier at Droplet Condensation. *Progress of Theoretical Physics Supplement* **184,** 400–414. doi:10.1143/PTPS.184.400 (2010).

37. Binder, K. Theory of first-order phase transitions. *Reports on Progress in Physics* **50,** 783–859. doi:10.1088/0034-4885/50/7/001 (1987).

38. Berg, B. *et al.* Properties of Interfaces in the two and three dimensional Ising Model. *Zeitschrift für Physik B Condensed ...* **239,** 229–239 (1993).

39. Lechner, W. *et al.* Role of the Prestructured Surface Cloud in Crystal Nucleation. *Physical Review Letters* **106,** 085701. doi:10.1103/PhysRevLett.106.085701 (2011).

40. Berg, B *et al.* Simulation of an ensemble with varying magnetic field: A numerical determination of the order-order interface tension in the D=2 Ising model. *Physical Review B* **47,** 497–500. doi:10.1103/PhysRevB.47.497 (1993).

41. Binder, K. Monte Carlo calculation of the surface tension for two- and three-dimensional lattice-gas models. *Physical Review A* **25,** 1699–1709. doi:10.1103/PhysRevA.25.1699 (1982).

42. Barber, C. B. *et al.* The quickhull algorithm for convex hulls. *ACM Transactions on Mathematical Software* **22,** 469–483. doi:10.1145/235815.235821 (1996).

43. Frigo, M. & Johnson, S. G. The Design and Implementation of FFTW3. *Proceedings of the IEEE* **93,** 216–231 (2005).

44. Agarwal, P. K. *et al.* in *Proceedings of the sixth annual symposium on Computational geometry - SCG '90* **422** (ACM Press, New York, New York, USA, 1990), 203–210. doi:10.1145/98524.98567.

45. Preparata, F. P. & Shamos, M. I. Computational Geometry: An Introduction (Monographs in Computer Science) (ed Gries, D.) (1985).

Clemens Moritz

Education

Since	**Master program Physics**, *University of Vienna.*
04/2011	Focus on Computational Physics.
10/2007-	**Bachelor program Physics**, *University of Vienna.*
04/2011	Finished with distinction in april of 2011.
1998-2006	**Secondary school**, *Bundesrealgymnasium Vienna 9.*

Bachelorthesis

Title	Performance Vergleich: C-Control vs. JX-Mega Board
Contents	Two microcontrollerboards based on ATMega microcontrollers have been compared with respect to their execution time of simple programs. Also some code abstracting low level functions of the controller has been developed for usage in lab courses.
Advisor	Ass.-Prof. Mag. Dr. Peter Steier, Isotope Research and Nuclear Physics, Faculty of Physics, University of Vienna

Masterthesis - In Preparation

Title	Geometric Phase Transitions in Periodic Boundary Conditions
Contents	In this work geometric phase transitions that are induced by the use of periodic boundary conditions in molecular simulations are studied in the 2D Ising model. In particular we have developed reaction coordinates for the slab-disc phase transition.
Advisor	Univ.-Prof. Mag. Dr. Christoph Dellago, Conputational Physics, Faculty of Physics, University of Vienna

Experience

Fall 2013 and	**Tutor**, *University of Vienna.*
Fall 2014	Tutor for a first year mathematics course at the faculty of physics.

Seitenberggasse 20/27 – 1160 Vienna, Austria
+43 699 194 76 883 • *clemensmoritz@gmx.at*

03/2009 - **Tutor**, *Schülerhilfe Humer GmbH.*
02/2013 Coaching for students from age six and up in mathematics and physics.

07/2006- **Paramedic**, *Red Cross Vienna.*
04/2007 Conscentious objector alternative service mostly in patient transport.

Skills

- Prior experience programming in C++, Fortran, Python, PHP and Java as well as in the usage of Unix-Like Systems and SQL databases.
- Extensive knowledge of physics and underlying mathematics.
- Long lasting experience in teaching of mathematics and physics to students.
- German as a first language.
- Good knowledge of written and spoken english.

Other Interests.

- Online Flightsimulation.

Since **Staffmember**, *VACC-Austria.*
12/2012 Tasked with technical issues such as development of the website and other software, server maintenance and provision of aviation data. VACC-Austria (`www.vacc-austria.org`) is an association that is part of a world wide flight simulation network called VATSIM (`www.vatsim.net`) and provides information and training for flight simulation enthusiasts in Austria and around the world.

- Snooker and Pool

Seitenberggasse 20/27 – 1160 Vienna, Austria
+43 699 194 76 883 • ✉ *clemensmoritz@gmx.at*